

## **Are internally observable vehicle data good predictors of vehicle emissions?**

Fernandes P. <sup>a\*</sup>, Macedo, E. <sup>a</sup>, Bahmankhah, B. <sup>a</sup>, Tomas, R. <sup>a</sup>, Bandeira, J.M. <sup>a</sup>, Coelho, M.C. <sup>a</sup>

<sup>a</sup>Department of Mechanical Engineering / Centre for Mechanical Technology and Automation (TEMA),  
University of Aveiro, Campus Universitário de Santiago, 3810-193 Aveiro – Portugal

\*Assistant Researcher, Mechanical Engineering, E-mail: [paulo.fernandes@ua.pt](mailto:paulo.fernandes@ua.pt)

### **ABSTRACT**

Scientific research has demonstrated that on-road exhaust emissions in diesel passenger vehicles (DPV) exceeds the official laboratory-test values. Increasing concern about the quantification of magnitude for these differences has meant an increasing use of Portable Emissions Monitoring System (PEMS), but the direct use of Internally Observable Variables (IOVs) can be useful to predict emissions.

The motivation for this paper is to develop an empirical approach that integrates second-by-second vehicle activity and emission rates for DPV. The objectives of this research are two-fold: 1) to assess the effect of variation in acceleration-based parameters, vehicle specific power (VSP) and IOVs on carbon dioxide

(CO<sub>2</sub>) and nitrogen oxides (NO<sub>x</sub>) emission rates; and 2) to examine the correlation between IOV-based predictors of engine load and VSP. Field measurements were collected from four DPV (two small, one medium and one multi-purpose) in urban, rural and highway routes using PEMS, GPS receivers and OBD scan tool, to measure real-world exhaust emissions and engine activity data.

Results suggest the relative positive acceleration (RPA) and mean positive acceleration (MPA) allowed a good differentiation with respect to route trips. IOVs models based on the product of manifold absolute pressure (MAP) and engine revolutions per minute (RPM), and VSP showed to be good predictors of emission rates. Although the CO<sub>2</sub> correlation was found to be good ( $R^2 > 0.8$ ), the models for NO<sub>x</sub> showed mixed results since some vehicles showed a reasonable correlation ( $R^2 \sim 0.7$ ) while others resulted in worst model predictions ( $R^2 < 0.6$ ).

IOVs models have potential to be integrated into vehicle engine units and connected vehicles, for instance, to provide real-time information on emissions rates, but other parameters regarding the thermal management on after treatment system must be included in NO<sub>x</sub> prediction. This would allow for a better understanding of true physics behind NO<sub>x</sub> emissions in DPV.

*Keywords:* Portable Emissions Measurement System; On-road emissions; Diesel; Internally Observable Variables; Vehicle Specific Power.

## 1. INTRODUCTION AND RESEARCH OBJECTIVES

Road traffic significantly contributes to urban air pollution as means of particulate matter (PM) and nitrogen oxides (NO<sub>x</sub>) emissions (EEA, 2018a). Between 1990 and 2015, transportation-related energy consumption increased by 25% in European Union (EU) (EEA, 2019b) in which road transportation and domestic aviation were the only transportation modes to report increases over this period, as their consumption rose by 23% and 4%, respectively (EU, 2017). Despite the deployment of clean powertrains, internal combustion engines are the most widely used technology in EU. Gasoline- and diesel-fueled represented around 56.7% and 35.9% of passenger cars sold in 2018, respectively (ACEA, 2019). On average, the carbon dioxide (CO<sub>2</sub>) of these cars were 120 g/km, which is clearly above the EU target of 95 g/km for 2020 (EEA, 2019a).

In view of persistent pollution in Europe, policy makers have been proposing stricter regulatory procedures either for emission standards or testing measurements (Commission Regulation (EC) No 692/2008, 2008). Thus, the so-called New European Driving Cycle (NEDC) was developed by the European Commission as part of the type approval process for homologating light duty vehicles (LDV) in Europe (Luján et al., 2018). Studies have been confirming a large discrepancy between measured NO<sub>x</sub> and respective emission limit in diesel passenger vehicles (DPV), certified according to Euro 2 up to Euro 6 standards (Degraeuwe and Weiss, 2017; Hooftman et al., 2018; Ntziachristos et al., 2016; Sileghem et al., 2014; Weiss et al., 2012). Similar results were found for CO<sub>2</sub> emissions; 10 to 20% in the gap between type-approval and real-world values (Fontaras et al., 2017).

To reduce such differences and to limit the adaptation of illegal strategies, the worldwide harmonized Light vehicles Test Procedure (WLTP) and complementary Real-Driving Emissions (RDE) were recently introduced in the EU legislation (EC, 2017). These procedures use Portable Emissions Measurement

Systems (PEMS) which allows quantifying real-world vehicle activity and emissions during a wide range of normal operating conditions (**Mahesh et al., 2018**).

As a result, a great deal of research has been conducted in Europe over the recent years to explore discrepancy between on-road and laboratory test emissions in diesel passenger vehicles (DPV) (**Chelsea Baldino et al., 2017; Kwon et al., 2017; Luján et al., 2018; O'Driscoll et al., 2018; Weiss et al., 2012**).

On-road emissions studies also have been performed worldwide in both gasoline passenger vehicles (GPV) (**Hu et al., 2016; O'Driscoll et al., 2018; Weiss et al., 2012; Yuan et al., 2019; Zhang et al., 2019**) and hybrid-electric vehicles (HEV) (**Holmén and Sentoff, 2015; O'Driscoll et al., 2018; Yang et al., 2019**). There is some research published concerning the impacts of driving behavior styles, such as the Relative Positive Acceleration (RPA), the Mean Positive Acceleration (MPA) and the product of acceleration and speed (**Gallus et al., 2017**), type and grade of roads (**Gallus et al., 2017; Yazdani Boroujeni and Frey, 2014; Zhang et al., 2019**) and ambient temperature conditions (**Gallus et al., 2017**) on gaseous exhaust emissions.

The major findings of above-mentioned studies are presented in **TABLE 1**. It can be observed that few studies carried out in on-road emissions have explored the concordance between internally observable variables (IOVs) and externally observed variables (EOVs) for predicting models for vehicle emissions on the basis of IOVs (**Hu et al., 2016**). On-road CO<sub>2</sub> and NO<sub>x</sub> emissions and fuel consumption are directly related to vehicle specific power – VSP (**Frey et al., 2008**), which takes into account kinetic energy, potential energy, rolling resistance and aerodynamic drag (**Jiménez-Palacios, 1999**). VSP is function of speed, acceleration and road grade. These variables can be categorized as EOVs (**USEPA, 2002**). A vehicle electronic control unit (ECU) via an On-board Diagnostic (OBD) interface measures, among others, real time revolutions per minute (RPM) and manifold absolute pressure (MAP), each of which can be categorized as IOVs. Previous studies suggested that, in some cases, models directly developed from

OBD data can provide better emission rates than VSP-based models, especially in high-emitting vehicles (Hu et al., 2016; Sandhu and Frey, 2013b). For instance, a VSP-based model for fuel use rate had coefficient of determination ( $R^2$ ) values ranged from 0.53 to 0.75. An IOV-based model developed based on the product of MAP and RPM had higher  $R^2$  (0.95-0.99). However, IOV-based models for low-emitting vehicles were not as good since a significant proportion of the measured concentrations was lower than the detection limit (Hu et al., 2016).

**TABLE 1** Key studies on emission measurements of DPV, LPV and HEV.

PEMS data collection for proof of concept and analysis can be costly. Besides, it is only applied to a few number of vehicles, making the upscaling of the results to an entire car fleet practically impossible. This has prompted the increased use of OBD scan tools in-vehicle data collecting. While there has been extensive work on the quantification of exhaust emissions for different DPV, research on developing predictive models for emissions based on IOVs is scarce (Asprion et al., 2013; d'Ambrosio et al., 2014). Since NO<sub>x</sub> is sensitive to the internal cylinder temperature estimation and accurate trapped mass assumptions (Desantes et al., 2012), any NO<sub>x</sub> modeling technique based on ECU data involves a trade-off between physics fidelity, calibration effort and computational cost (Guardiola et al., 2014).

For diesel engines, not only engine load and engine revolutions influence NO<sub>x</sub> emissions, but also the exhaust after-treatment system such as Lean NO<sub>x</sub> Trap (LNT) and Selective Catalytic Reduction (SCR) (Johnson, 2016). To achieve the next emissions standards, high NO<sub>x</sub> conversion efficiency in the after treatment system in the SCR system is required (Bai et al., 2017; Giechaskiel et al., 2014). NO<sub>x</sub> reduction by SCR catalysts is affected by a wide range of factors, such as variations in the NO<sub>2</sub>/NO<sub>x</sub> ratio, which

are caused by oxidation catalysts such as the diesel oxidation catalyst and diesel particulate filter installed in diesel engines (Cho et al., 2017), ammonia (NH<sub>3</sub>) to NO<sub>x</sub> ratio (Seneque et al., 2015) and catalytic temperature (Bai et al., 2018). NO<sub>x</sub> conversion of these systems is sensitive by the catalytic temperature rather than the other factors (Ahari et al., 2015). For instance, NO<sub>x</sub> emissions rates notably increases if the exhaust temperature is lower than 200°C, and there is a sudden application of load (e.g., hill or acceleration). The exhaust temperature under low speeds and low load in urban conditions is mostly below 300 °C. If the load is close to the maximum, then the exhaust temperatures can exceed 500°C (Seneque et al., 2015). Indeed, control strategies to improve NO<sub>x</sub> emissions in lower temperature conditions for SCR are of high interest (Guardiola et al., 2017; Hu et al., 2017; Liu and Lee, 2018).

This research develops a second-by-second methodology that integrates vehicle activity and on-road emission rates for DPV. The paper considered two hypotheses as follows: i) IOV-based model is a good predictor of CO<sub>2</sub>, regardless of the driving conditions and vehicle; ii) NO<sub>x</sub> model only based on load variables are worse predictive of NO<sub>x</sub> exhaust emissions in diesel engines. These predictions were tested in one mix urban and rural route and two highway routes, with variations in traffic volumes. Driving style was also characterized by metrics for both validating PEMS trips and examining their impacts on emissions rates.

Therefore, the specific research objectives were: 1) to assess the effect of variation in RPA, MPA and the 95th percentile of the product of speed and positive acceleration greater than 0.1 m.s<sup>-2</sup> –  $va_{pos\_}[95]$ , VSP and vehicle engine variables on CO<sub>2</sub> and NO<sub>x</sub> emission rates; and 2) to explore the correlation between IOV-based predictors of engine load and VSP. This article contributes to the state-of-art advancement in the two main aspects:

- To characterize real-world emission factors for both global and local pollutants for different DPV on different types of road configurations;

- To develop predictive models based on IOVs and EOVs for different diesel vehicle categories in Europe.

## 2. METHODOLOGY

This paper focused on hot stabilized tailpipe exhaust emissions from DPV using an integrated PEMS, OBD and GPS receivers over test routes that fulfills the main requirements imposed by the RDE regulation (Kwon et al., 2017). In the next sections, methodology steps pertaining to experimental design (Section 2.1), instruments and test conditions (Section 2.2), field measurements (Section 2.3) quality assurance (Section 2.4), and data analysis (Section 2.5) are explained in detail.

### 2.1. Experimental design

Field measurements of four DPVs – two small cars, one medium car and one multi-purpose car (EC, 1999) – were conducted. These vehicles varied in emission standards, category, engine displacements and mileage, as listed in TABLE 2. The distribution of engine sizes (1.2 L – 1.8 L) in the test fleet was representative of the European market (ACAP, 2017). Testing vehicles V2-V4 were type approved to the Euro 6-b standard, thus they are not designed to meet on-road limits. V2 and V4 are equipped with passive SCR while V3 has an active SCR with urea dosing.

**TABLE 2** Technical specifications of the test vehicles.

The on-road emissions tests were carried out in Aveiro region (Portugal), along the routes (R1, R2 and R3) in both directions of travelling (A→B→A), as depicted in **FIGURE 1**. The routes were designed to include a wide range of European on-road driving conditions such as speed range, acceleration-deceleration profiles, traffic conditions and altitude profiles (**EC, 2017**). R1 (23.6 km) is a mix of rural (77%) and urban (23%) roads with one lane, and it has 12 roundabouts, 14 traffic lights and one stop-controlled intersection (North-South direction) throughout its length. More than half of both R2 (30.2 km) and R3 (34.1 km) is on low-traffic-volume and high-traffic toll highway sections, respectively. Average daily traffic (ADT) on R2 and R3 highway study segments is about 11 700 and 39 950, respectively (**IMT, 2019**). Although all routes are located in flat areas for which road grades are negligible, R2 and R3 contain some elevation differences in some stretches, as shown in **FIGURE 2**.

**FIGURE 1** Routes aerial view. Background Map Source [Open Street Maps].

**FIGURE 2** Test routes: a) altitude profiles; and b) typical speed distributions.

## **2.2. Instruments and Test Conditions**

The 3DATX ParSYNC integrated PEMS (iPEMS) (**3DATX, 2018**) was used to perform on-road emissions tests of a limited number of gaseous exhaust constituents. The 3DATX has developed parSYNC® integrated PEMS (iPEMS) with 3.7kg of weight (including batteries) which is capable of measuring CO<sub>2</sub> (in volume fraction), NO, NO<sub>2</sub>, and the particulate number (PN) at a frequency of 1 Hz. The system uses a replaceable Sensor Cartridge to obtain real-time PM/PN and GasMOD™ Sensor Cartridge for NO<sub>x</sub> (with a range of 0 – 5 000 ppm) and CO<sub>2</sub> (with a range of 0 – 20%) (**3DATX, 2018**).



**TABLE 3** summarizes the measurements principles and sample condition of the equipment.

**TABLE 3** Measurements Principles and Sample Condition of the selected PEMS.

### 2.3. Field Measurements

One complete PEMS trip duration was between 100 and 120 minutes since the internal battery can power the unit for over three hours. A temperature/pressure sensor monitored environment parameters (Ambient Temperature – T, Humidity – H), and a QSTARZ GPS Travel Recorder (absolute position accuracy: 3 m) continuously logged vehicle position and elevation. The OBD-II ELM327 measured main car engine data, such as speed, mass air flow (MAF), MAP, RPM and intake air temperature (IAT). For all vehicles, the fuel flow rate (FFR) was also reported by the OBD. **TABLE 4** lists data used in these monitoring campaigns, including variability in measured data by vehicle type and observed ranges of above parameters.

**TABLE 4** Summary of ambient and activity real-world data for selected vehicles operated on R1, R2 and R3 routes (both directions of travelling).

All measurements were carried out in September, October and November 2018 and within an overall ambient temperature range of 12 – 18 °C. All trips were performed with different drivers to capture different driving styles. Since the toll plaza in R3 has conventional and electronic pay tolls, measurements were conducted for both facilities. For each vehicle, more than 10 000 seconds of valid PEMS, OBD and GPS data were collected. It should be mentioned that the start-stop system was deactivated before starting

route tests due to the fact the iPEMS needs continuously an energy source power during measurements. On average, idle situations lasting more than 5 seconds accounted for 2% of total route-specific travel time.

#### **2.4. Data processing and Quality Assurance**

Data processing and quality assurance focused on the following steps (**Delavarrafiee and Frey, 2018; Sandhu and Frey, 2013a**): 1) to collect OBD data on a second-by-second; 2) to synchronize data from PEMS, GPS and OBD into one database; and 3) to check data screening to correct or remove data errors. Characteristic errors include unusual MAF, RPM and MAP values that remained constant indicating that the data were no longer being updated and negative CO<sub>2</sub>, NO and NO<sub>2</sub> values. Both the errors were corrected, and errant data values were screened out for data analysis.

#### **2.5. Data Analysis**

Each vehicle trip of R1, R2 and R3 routes was extracted and separated for comparison. This ensured consistency in the assessment of trip-specific characteristics (**Yazdani Boroujeni and Frey, 2014**), such as RPA, MPA,  $va_{pos\_}[95]$ , emissions, VSP and IOVs.

##### ***2.5.1. Verification of the trip validity***

Driving parameters were calculated to characterize the driving profile of the PEMS route trips. For acceleration based parameters, the acceleration  $a_i$  in the second of travel  $i$  in  $m.s^{-2}$  was calculated from OBD speed, as expressed by Equation 1 (**EC, 2016**):

$$a_i = \frac{v_{i+1} - v_{i-1}}{2 \times 3.6}, \quad (1)$$

where  $v_{i-1}$  and  $v_{i+1}$  are the vehicle instantaneous speed in the second of travel  $i-1$  and  $i+1$ , respectively (km.h<sup>-1</sup>).

The 95th percentile of the product of vehicle speed and positive acceleration,  $va_{\text{pos\_}}[95]$ , is the metric for evaluating the maximum dynamic boundary conditions in the Commission Regulation (EU) 2017/1151 of 1 June 2017 (EC, 2017); if the  $va_{\text{pos\_}}[95]$  is below a certain value, then a PEMS trip is valid in the RDE procedure. RPA is the metric for assessing the minimum dynamic boundary conditions in prior regulation; if a PEMS trip has RPA above a certain value, then it is valid in the RDE procedure. Therefore, only PEMS trips that fulfilled the above-mentioned criteria were selected for this emission analysis. More details about the validation of RDE procedure can be found in (EC, 2017).

The above parameters RPA (in m.s<sup>-2</sup>), MPA (in m.s<sup>-2</sup>) and  $va_{\text{pos\_}}[95]$  (m<sup>2</sup>.s<sup>-3</sup>) were then, calculated according to Equations 2, 3 and 4, respectively (EC, 2017):

$$RPA = \frac{\sum_i \frac{v_i}{3.6} \times a_i^+}{d}, \quad (2)$$

$$MPA = \text{mean}(a_i^+), \quad (3)$$

$$va_{\text{pos\_}}[95] = P95\left(\frac{v_i}{3.6} \times a_i^+\right), \quad (4)$$

where  $a_i^+$  represents the positive values of the acceleration greater than 0.1 m.s<sup>-2</sup> for the second of travel  $i$  (m.s<sup>-2</sup>),  $d$  is the total distance of the route (m) and  $P95$  corresponds to the 95th percentile.

### 2.5.2. Road grade calculation

The methodology for road grade calculation followed a two-step procedure, consisting of (i) correction of instantaneous vehicle altitude data, and (ii) the calculation of the cumulative positive elevation gain.

Although the GPS device was provided data without any observable signal loss, the second-by-second altitude data were acquired from the topographic map (ERSI, 2016). In addition, each instantaneous altitude data was corrected under the conditions given in Equation 5 (EC, 2017):

$$\bar{h}_i = \begin{cases} h_{i-1}, & \text{if } |h_i - h_{i-1}| > \frac{v_i}{3.6 \times \sin 45^\circ}, \\ h_i, & \text{otherwise,} \end{cases} \quad (5)$$

where  $\bar{h}_i$  is the corrected altitude,  $h_i$  and  $h_{i-1}$  are the altitude in the second of travel  $i$  and  $i-1$ , respectively (m above sea level).

These values were used for the calculation of the cumulated altitude gain in meters, as shown in Equation 6 (Gallus et al., 2017):

$$altgain = \sum_i \Delta \bar{h}_i \text{ for } \Delta \bar{h}_i > 0, \quad (6)$$

To quantify road grade with enough precision at every location along a route, a segment method proposed by Yazdani Boroujeni and Frey (2014) was used. First, the entire route trip was divided into multiple segments of a constant length, then the road grade was calculated using linear regression through all altitude data. This increases the statistically accuracy of the calculated road grade, since data from several trips over the same route are combined (Yazdani Boroujeni and Frey, 2014).

Thus, a segment length of 100 m was chosen as the best trade-off between the number of GPS data points per segment (small number decreases the reliability of the calculated road grade) and extremely large segment length (too long means inappropriate smoothed out grade variations). The segment method was applied to PEMS trips conducted with all vehicles on routes R1, R2 and R3, thereby resulting in the following positive cumulative elevation gains: 59 meters/100 km (R1) 167 meters/100 km (R2) and 132 meters/100 km (R3).

### 2.5.3. Emission Rates

Because the parSYNC does not measure exhaust flow, a general procedure was followed to compute pollutant mass at each second of operation using the method based on the Regulatory Information 40 CFR 86.144 for exhaust emissions (EPA, 2018). The generic form of an equation was developed using the simple proof given by Equation 7 (Leland and Stanard, 2018):

$$\dot{m}_{\text{ex}} = MAF + FFR \cdot \rho_{\text{fuel}}, \quad (7)$$

where  $\dot{m}_{\text{ex}}$  is the exhaust mass flow rate ( $\text{g}\cdot\text{s}^{-1}$ ),  $MAF$  is the mass air flow rate ( $\text{g}\cdot\text{s}^{-1}$ ),  $FFR$  is the fuel flow rate ( $\text{L}\cdot\text{s}^{-1}$ ) and  $\rho_{\text{fuel}}$  is the fuel density ( $\text{g}\cdot\text{L}^{-1}$ ).

For the purpose of analyses, the sum of concentration signals for NO and NO<sub>2</sub> corresponds to the NO<sub>x</sub> concentration. For CO<sub>2</sub> and NO<sub>x</sub> mass emission rate calculations, the following equations were used (EPA, 2018):

$$m_{\text{CO}_2} = \dot{V}_{\text{ex}} \rho_{\text{CO}_2} X_{\text{CO}_2}, \quad (8)$$

$$m_{\text{NO}_x} = \dot{V}_{\text{ex}} \rho_{\text{NO}_x} X_{\text{NO}_x} \frac{1}{1 - 0.0047(H - 75)}, \quad (9)$$

where  $m_{\text{CO}_2}$  is the mass flow rate of  $\text{CO}_2$  ( $\text{g}\cdot\text{s}^{-1}$ ),  $\dot{V}_{\text{ex}}$  is the exhaust volumetric flow rate (corrected to standard conditions) ( $\text{m}^3\cdot\text{s}^{-1}$ ),  $\rho_{\text{CO}_2}$  is the density of  $\text{CO}_2$  at the standard conditions ( $\text{g}\cdot\text{m}^{-3}$ ) and  $X_{\text{CO}_2}$  is the volume fraction of  $\text{CO}_2$  (%),  $m_{\text{NO}_x}$  is the mass flow rate of  $\text{NO}_x$  ( $\text{g}\cdot\text{s}^{-1}$ ),  $\rho_{\text{NO}_x}$  is the density of  $\text{NO}_x$  at the standard conditions ( $\text{g}\cdot\text{m}^{-3}$ ),  $X_{\text{NO}_x}$  is the volume fraction of  $\text{NO}_x$  (ppm) and  $H$  is the humidity (%).

#### 2.5.4. Uncertainty Considerations

As mentioned previously in **Section 2.5.3**, the exhaust flow rate was estimated based on engine MAF and FFR reported via the OBD interface. Thus, the uncertainty of exhaust emissions was based on imprecisions of MAF and FFR measurements,  $\text{CO}_2$ ,  $\text{NO}$  and  $\text{NO}_2$  analyzers and trip distance measurements. Routine calibrations of gas analyzers (controlling for zero and span drift once per trip) were performed prior each test using the UN 1956 gas mixture to mitigate measurements errors of iPEMS. For the estimation of the emissions uncertainty (in relative terms), the propagation rule for multiplication and division in the form of Equation 10 (**Farrance and Frenkel, 2012**) was used:

$$\varepsilon_{E,j} = k \left( \sqrt{\varepsilon_{\text{MAF}}^2 + \varepsilon_{\text{FFR}}^2 + \varepsilon_{\phi}^2 + \varepsilon_d^2} \right), \quad (10)$$

$$\varepsilon_{\phi}^2 = \begin{cases} \varepsilon_{\text{CO}_2}^2, & \text{if } j = \text{CO}_2 \\ \varepsilon_{\text{NO}}^2 + \varepsilon_{\text{NO}_2}^2, & \text{otherwise} \end{cases}$$

where  $\varepsilon_{E,j}$  is the relative expanded uncertainty of specie  $j \in J$ ,  $J = \{\text{CO}_2, \text{NO}_x\}$  (%);  $k$  is the coverage factor (= 2 for a confidence interval of 95%);  $\varepsilon_{\text{MAF}}$  is the relative uncertainty of the MAF sensor (%);  $\varepsilon_{\text{FFR}}$

is the relative uncertainty of the FFR sensor (%);  $\varepsilon_\phi$  is the relative uncertainty of the gas analyzer (%); and  $\varepsilon_d$  is the relative uncertainty of the trip distance (%).

To obtain the uncertainty of each component of the Equation 10, the technical specifications in the RDE regulation and experimental data were considered. The uncertainty of gas analyzers is determined by the accuracy (at a given concentration value), drift over time for zero and maximum concentrations (span), and linearity (standard error requirement) (**Giechaskiel et al., 2018**). In addition, the uncertainty is influenced by the time delay of signals, effect of environmental conditions (e.g., altitude and temperature), uncertainty of the regulated laboratory constant-volume sampling (CVS) and zero drift of the analyzer. Equation 11 provides the absolute uncertainty for an emission level (**Giechaskiel et al., 2018**):

$$\delta_{F,E,j} = (\varepsilon_{E,j} + \varepsilon_t + \varepsilon_B - \varepsilon_{CVS}) L_j + \delta_{drift}, \quad (11)$$

where  $\delta_{F,E,j}$  is the absolute uncertainty of specie  $j$  (g.km<sup>-1</sup>),  $\varepsilon_{E,j}$  is the relative uncertainty of specie  $j$ ;  $\varepsilon_t$  is the time misdealing of signals (%),  $\varepsilon_B$  is the effect of test conditions (%),  $\varepsilon_{CVS}$  is the uncertainty of the regulated CVS (%),  $L_j$  is the emission level of specie  $j$  (g.km<sup>-1</sup>), and  $\delta_{drift}$  is the uncertainty associated with the zero drift (g.km<sup>-1</sup>).

The small sample size together to the lack of laboratory tests resulted in few data to perform a reliable uncertainty analysis of iPEMS setup. For this reason, the authors used values from the 2017 margins review study (**Giechaskiel et al., 2018**), as presented in **TABLE 5**. The assessment of uncertainly in this case considered conservative values taken under realistic conditions. For purpose of the analysis, the

contribution of the zero drift was negligible because analyzer was brand new and calibrated. Using these values, the final uncertainty of CO<sub>2</sub> and NO<sub>x</sub> is 33% and 35%, respectively.

**TABLE 5** Summary of uncertainty values used in this study (EC, 2016; Giechaskiel et al., 2018).

### 2.5.5. *Concordance between IOVs and EOVs*

To evaluate the concordance between IOVs and EOVs as indicators of engine power demand, the relationship between the product of MAP and RPM ( $P_{MAP \times RPM}$ ), and VSP was explored. Emission rates can be stratified into bins by using VSP to represent any driving cycle. The use of bins enables quantification of linear or nonlinear trends without the need of fitting a parametric function to the data, which often introduces model bias (Sandhu and Frey, 2013a). VSP is a useful explanatory variable for emissions since it accounts for kinetic energy, aerodynamic drag, tire rolling resistance and road grade. Equation 12 applies VSP using parameter values to specific case of a typical DPV (USEPA, 2002):

$$VSP_i = v_i [1.1a_i + 9.81r + 0.132] + 0.000302.v_i^3, \quad (12)$$

where  $VSP_i$  is the Vehicle Specific Power in the second of travel  $i$  (kW.ton<sup>-1</sup>) and  $r$  is the road grade (slope).

Each second-by-second estimate of VSP was stratified into 14 bins and the average CO<sub>2</sub> and NO<sub>x</sub> emission rates for each bin were estimated. These modes are typically in DPV (USEPA, 2002).

Although the engine air flow is influenced by IAT, engine displacement or engine volumetric efficiency, MAP and RPM tend to have much more relative variability for a given engine with fixed engine



displacement and number of strokes per cycle (**Charles Fayette, 1985**). Typically the variability in emission rates are better explained by  $P_{MAP \times RPM}$  than MAP and RPM separately (**Hu et al., 2016**). Accordingly, relationships between emission rates ( $CO_2$  and  $NO_x$ ) and  $P_{MAP \times RPM}$  were examined. Studies have been showing a correlation of emissions and  $P_{MAP \times RPM}$  describing power-shaped curves (**Charles Fayette, 1985; Hu et al., 2016**). For this reason, a model in the form of Equation 13 was used:

$$m_{j,w,pred} = c \left( P_{MAP \times RPM} \right)^n, \quad (13)$$

where  $m_{j,w,pred}$  is the predicted mass flow rate of specie  $j$  and vehicle  $w \in W$ ,  $W = \{V1, V2, V3, V4\}$ ,  $c$  is the fitted scaling parameter and  $n$  is the power parameter.

However, Equation 13 as it stands is not complete, as the transform of the error term has been omitted, i.e., bias is introduced in the transformation back from the logarithm unit to the original arithmetic unit. To overcome this issue, a log-transformation bias correction factor was used following the method demonstrated by **Newman (1993)**, as follows:

$$m_{j,w,pred,cor} = c C_{\log} \left( P_{MAP \times RPM} \right)^n, \quad (14)$$

where  $m_{j,w,pred,cor}$  is the corrected predicted mass flow rate of specie  $j$  and vehicle  $w$ , and  $C_{\log}$  represents a log-transformation bias correction factor.

Since a log-transformation leads to an estimate of the median value, an additional bias correction is needed by using a linear regression between predicted emission rates by Equation 12 and measured emission rates, as indicated in Equation 15:

$$m_{j,w,pred,cor} = a' \cdot m_{j,w,measure} + b', \quad (15)$$

where  $m_{j,w,measure}$  is the measured mass flow rate of specie  $j$  and vehicle  $w$ , the  $a'$  represents the fitted slope, and  $b'$  is the model intercept.

Considering the above-mentioned steps, the final form in predicting emission rates of CO<sub>2</sub> and NO<sub>x</sub> on the basis of  $P_{MAP \times RPM}$  is rewritten as:

$$m'_{j,w,pred,cor} = c \frac{C_{log}}{a'} (P_{MAP \times RPM})^n - \frac{b'}{a'} \quad (16)$$

where  $m'_{j,w,pred,cor}$  is the corrected predicted mass flow rate of specie  $j$  and vehicle  $w$ .

### 3. RESULTS

In this section, the main results from driving behavior parameters are presented and discussed (**Section 3.1**). The average emissions per kilometer by vehicle are compared among routes in **Section 3.2** followed by the presentation and discussion of the fitted models for EOVs and IOVs in **Section 3.3**.

#### 3.1. Driving style

In **FIGURE 3** all second-by-second acceleration were plotted against vehicle speed (OBD) for all trips on a same route. As suspected, R1 covered a wide acceleration and deceleration values when compared to other routes. This can be explained by the fact that test vehicles faced multiple stops as they approach through traffic lights and roundabouts along R1, and as result they had sharper accelerations and decelerations rates. The scatter plots also indicated differences in acceleration-speed conditions between

R2 and R3 for vehicle speeds below 25 km/h. These results occurred for two main reasons: 1) conventional pay tolls at R3 (vehicles must come a complete stop and undergone several stop-and-go episodes until the payment is completed, thus resulting in acceleration at low speeds); and 2) low traffic along R2 highway trip section (see **Section 2.1**) together with an electronic pay toll system where no stopping is required. By contrast, R2 and R3 trips at speeds around 25-125 km/h covered a wider band of acceleration and speed combinations.

**FIGURE 3** Acceleration as a function of vehicle speed: a) R1; b) R2; and c) R3.

**FIGURE 4** shows an overview of the acceleration-based parameters RPA and MPA by route. The bar height represents the mean of the respective parameter for different trips while the range bar represents the standard deviation. Both parameters indicated a good differentiation with respect to routes. The average RPA in R2 was 22% and 25% lower than the corresponding value for routes R3 and R1, respectively. R3 yielded the highest MPA (perhaps due to the higher capacity of R3 that allow for more overtaking maneuvers), but R1 has a larger standard deviation bandwidth (possibly due to the variations in acceleration rates faced by vehicles after stopping in traffic light, roundabout or crosswalk). The resulting coefficients of variability of average MPA ranged from 0.12 to 0.23 between R1 and R3.

**FIGURE 4** Driving dynamics of the PEMS trips: a) RPA by route; and b) MPA by route.

**FIGURE 5** exhibits the 95<sup>th</sup> percentile of the  $va_{pos\_}[95]$  and RPA as function of the average speed of each trip. The dashed diagonal line represents the threshold values for above metrics that were taken from the

current RDE regulation draft (EC, 2017). Almost data points fell below this line showing trips in this study met the  $va_{pos\_}[95]$  RDE dynamic boundary conditions. There was an exception in one trip along R3 that was further removed from emission analysis. The results also show all data points in this study fell above the corresponding dash diagonal line, thereby fulfilling RDE dynamic boundary conditions (EC, 2017).

**FIGURE 5** Validation of PEMS trips: a)  $va_{pos\_}[95]$  by speed; and b) RPA by speed.

### 3.2. Test route emissions

This section presents the average CO<sub>2</sub> and NO<sub>x</sub> emissions per kilometer for the different routes and separated for different vehicles. The following density values of CO<sub>2</sub> and NO<sub>x</sub> were used (Leland and Stanard, 2018):  $\rho_{CO_2} = 1\,830\text{ g.m}^{-3}$ ;  $\rho_{NO_x} = 1\,913\text{ g.m}^{-3}$ . A diesel density value  $\rho_{fuel}$  of  $835\text{ g.L}^{-1}$  was used (Engineering ToolBox, 2019).

From **FIGURE 6**, it can be observed that the R2 and R3 produced the highest CO<sub>2</sub> and NO<sub>x</sub> per trip distance. There was a greater difference between R2/R3 and R1 emissions per unit distance in CO<sub>2</sub> (between 9% and 23%, depending on the vehicle) than for NO<sub>x</sub> (between 11% and 178%, depending on the vehicle). The standard deviation bars also confirmed that the variability within each route type was substantial (up to 32% and 63% for CO<sub>2</sub> and NO<sub>x</sub>, respectively). Owing to their engine power, high-sized V1 and V3 generated the highest amount of CO<sub>2</sub> emissions, regardless of the type of route. Although V2 and V4 (S-category, as presented in **TABLE 2**) vehicles achieved similar CO<sub>2</sub> performance, V2 generated an average amount of NO<sub>x</sub> emissions per unit distance 38% higher than V4 did. This point can be explained by the high mileage (7 000 km) and lifetime of V2 as compared with V4, thus causing a

deterioration in the SCR system (**EEA, 2016, 2018b**). A close analysis allows to confirm on-road CO<sub>2</sub> surpassed vehicle type-approval in 64% and 105% between V1 and V3. Also, Euro 6 vehicles were out of compliance with respective NO<sub>x</sub> emission limit [see conformity factors of Euro 6-b post 2015 vehicles in **White et al. (2018)**], with emissions ranging from 3 to 4 times higher on average. Nevertheless, testing vehicles are pre-RDE DPV, i.e., they are only tested in a laboratory over the NEDC driving cycle.

**FIGURE 6** Average emissions (with standard deviation values) by vehicle and route: a) CO<sub>2</sub> per unit distance; and b) NO<sub>x</sub> per unit distance.

Results confirm that due to the difference route types there is a difference in CO<sub>2</sub> and NO<sub>x</sub> emissions for each car, even for those of the same engine standard and vehicle category. All vehicles had emissions far in exceedance of approval values which is in accordance with prior studies (e.g., (**Chelsea Baldino et al., 2017**)). Because of limited number of PEMS runs, the different trips had high variability in emissions. Therefore, there is a need for a suitable methodology capable of predicting emission rates on the basis of VSP and IOVs.

### **3.3. Summary of regression models**

For each of the 4 vehicles, the relationship between emission rates, EOVs and IOVs was explored. The models were calibrated based on 70% of the available data sets (training) (**Liu et al., 2017**), while remaining data (testing) were withheld for model validation. It must be emphasized that these are stratified samples.

### 3.3.1. IOVs versus VSP

Average  $P_{MAP \times RPM}$  values were plotted against VSP, ranging from -30 to 30 kW/ton in 1-kW/ton intervals, as displayed in **FIGURE 7**. This range represents almost 98% of vehicle's activity data. Since no load at engine is observed at negative VSP, the  $P_{MAP \times RPM}$  values did not follow a power trend over vehicle specific power. At positive VSP, the product of MAP and engine RPM increased monotonically assuming a power relation; the adjusted  $R^2$  values for V1, V2, V3 and V4 were 0.89, 0.88, 0.80 and 0.82, respectively. The  $p$ -values for the power and scaling parameters were both less than  $1 \times 10^{-11}$ , indicating statistical significance. The main conclusions derived from **FIGURE 7** are that the product of MAP and engine RPM is a good proxy for engine power demand for the above diesel vehicles.

**FIGURE 7** Measured  $P_{MAP \times RPM}$  versus VSP, with 1-kW/ton intervals, by vehicle: a) V1 – VSP<0; b) V1 – VSP>0; c) V2 – VSP<0; d) V2 – VSP>0; e) V3 – VSP<0; f) V3 – VSP>0; g) V4 – VSP<0; and h) V4 – VSP>0.

### 3.3.2. Emission rates versus VSP

**FIGURE 8** exhibits the potential of the VSP-based approach within each bin for predicting CO<sub>2</sub> and NO<sub>x</sub> emission rates by vehicle. Results showed a very good fit ( $R^2 > 0.92$ ) between predicted and observed CO<sub>2</sub> using linear regression analysis. The findings for NO<sub>x</sub> were generally not as good as those for CO<sub>2</sub>; the predicted  $R^2$  for V1, V2, V3 and V4 were 0.83, 0.75, 0.83 and 0.78, respectively. The scatter plots also confirmed predicted values far from observed data in high emission rates, i.e., high VSP bins, which may be explained to the small size of dataset. Notwithstanding these differences and variability in measured

rates (size of the error bars), VSP-modal approach showed to be accurate in estimating the mean trend in both CO<sub>2</sub> and NO<sub>x</sub>.

**FIGURE 8** Comparison between measured and predicted emission rates based on VSP-modal approach, by vehicle: a) V1 – CO<sub>2</sub>; b) V1 – NO<sub>x</sub>; c) V2 – CO<sub>2</sub>; d) V2– NO<sub>x</sub>; e) V3 – CO<sub>2</sub>; f) V3 – NO<sub>x</sub>; g) V4 – CO<sub>2</sub>; and h) V4 – NO<sub>x</sub>.

### 3.3.3. Emission rates versus IOVs

The relationship between CO<sub>2</sub> emissions rates (using training set) and the product of MAP and RPM are shown in **FIGURE 9**. Scatter plots indicated that most of data points followed a power trend (adjusted  $R^2$  values for CO<sub>2</sub> as a power function of  $P_{MAP \times RPM}$  ranged from 0.46 to 0.74, depending on the vehicle) (**FIGURE 9**). These models had  $p$ -values lower than 0.05 in both power and scaling parameters indicating thus statistical significance. After bias correction (Equations 14 and 15), the predicted CO<sub>2</sub> in terms of  $P_{MAP \times RPM}$  using Equation 16 is as follows:

$$m'_{CO_2, V1, pred, cor} = 1.89 \times 10^{-8} \times P_{MAP \times RPM}^{1.54} - 0.57 \quad (R^2 = 0.65, Fsig < 0.01) \quad (17)$$

$$m'_{CO_2, V2, pred, cor} = 1.42 \times 10^{-7} \times P_{MAP \times RPM}^{1.38} - 0.81 \quad (R^2 = 0.46, Fsig < 0.01) \quad (18)$$

$$m'_{CO_2, V3, pred, cor} = 2.12 \times 10^{-9} \times P_{MAP \times RPM}^{1.72} - 0.32 \quad (R^2 = 0.74, Fsig < 0.01) \quad (19)$$

$$m'_{CO_2, V4, pred, cor} = 2.18 \times 10^{-6} \times P_{MAP \times RPM}^{1.41} - 0.69 \quad (R^2 = 0.72, Fsig < 0.01) \quad (20)$$

**FIGURE 9** CO<sub>2</sub> emission rates versus IOVs, by vehicle: a) V1; b) V2; c) V3; and d) V4.

Albeit reasonable, a model on the basis of  $P_{MAP \times RPM}$  worse explained the variability in NO<sub>x</sub> emission rates; the adjusted  $R^2$  values for V1, V2, V3 and V4 were 0.54, 0.34, 0.71 and 0.44, respectively. There was cluster of data in which measured emission rates were much higher than the values predicted by fitted model. The most possible reason for these differences might be the ECU that is switching from a close- to an open-loop operation to keep the engine from overheating. Nevertheless, it must always be borne in mind that these short-duration events represent different operating conditions than those obtained in majority of data set (**Charles Fayette, 1985**). Since a model based on the basis of  $P_{MAP \times RPM}$  was not able to predict this cluster of very high emissions (only 0.3% of travel time), data were stratified for NO<sub>x</sub> emission rates less than  $0.3 \text{ g.s}^{-1}$ . For each vehicle, the IOV model based on  $P_{MAP \times RPM}$  was developed in the same way than the model for CO<sub>2</sub>. After bias correction (Equations 14 and 15), the predicted NO<sub>x</sub> in terms of  $P_{MAP \times RPM}$  in the form of Equation 16 can be given by:

$$m'_{NOX,V1,pred,cor} = 1.57 \times 10^{-11} \times P_{MAP \times RPM}^{1.76} - 0.01 \quad (R^2 = 0.54, Fsig < 0.01) \quad (21)$$

$$m'_{NOX,V2,pred,cor} = 1.30 \times 10^{-11} \times P_{MAP \times RPM}^{1.80} - 0.01 \quad (R^2 = 0.34, Fsig < 0.01) \quad (22)$$

$$m'_{NOX,V3,pred,cor} = 3.47 \times 10^{-17} \times P_{MAP \times RPM}^{2.72} \quad (R^2 = 0.71, Fsig < 0.01) \quad (23)$$

$$m'_{NOX,V4,pred,cor} = 4.50 \times 10^{-8} \times P_{MAP \times RPM}^{1.35} - 0.01 \quad (R^2 = 0.45, Fsig < 0.01) \quad (24)$$

**FIGURE 10** NO<sub>x</sub> emission rates versus IOVs, by vehicle: a) V1 b) V2; c) V3; and d) V4.



To assess the goodness of fit, a comparison between IOVs based and measured emission rates was illustrated in **FIGURE 11**. The standard deviation of residuals was small compared with mean emission rates. They represented less than 40% and 60% of mean measured CO<sub>2</sub> and NO<sub>x</sub>, respectively. When look at CO<sub>2</sub>, the predicted values of  $R^2$  for IOVs based models versus measured rates ranged from 0.87 to 0.92, which is similar to the values obtained with EOV-based models. The scatterplots clearly indicated high variation in the residual errors, which is mostly explained by small sample size in high emission rates. The relationship between emission rates predicted by Equations 21 to 24 and measured NO<sub>x</sub> emission rates in high-sized V1 and V3 showed a better fit ( $R^2 > 0.70$ ) than for small cars ( $R^2 < 0.60$ ). Although the graphs suggest weak fitted models in some vehicles, there are several data points clustered close to the fitted line.

**FIGURE 11** Comparison between measured and predicted emission rates based on IOV-based model, by vehicle: a) V1 – CO<sub>2</sub>; b) V1 – NO<sub>x</sub>; c) V2 – CO<sub>2</sub>; d) V2– NO<sub>x</sub>; e) V3 – CO<sub>2</sub>; f) V3 – NO<sub>x</sub>; g) V4 – CO<sub>2</sub>; and h) V4 – NO<sub>x</sub>.

#### **3.3.4. Discussion**

The findings from above sub-sections confirmed the first hypothesis of the paper regarding the relationship between IOVs and CO<sub>2</sub> emission rates. The model based on the product of RPM and MAP showed to be accurate in predicting CO<sub>2</sub> emission rates on a second-by-second basis. Since this gas is a good surrogate of fuel use rates, such approach can be applied to estimate vehicle-specific fuel use.

The second hypothesis of the paper was also confirmed, i.e., the developed models based on load parameters had a fair performance in predicting NO<sub>x</sub> emission rates, especially in light vehicles. This is

possible due to other IOVs that are not included in the developed models whose impact in NO<sub>x</sub> conversion rates in SCR system are relevant. Another reason may be the short gear shift of V2 and V4 compared with high-sized C, thus, generating clusters of high emissions during gear selection.

It is worth noting an IOV model simply based on RPM and MAP cannot incorporate, per se, all factors with impacts on NO<sub>x</sub> emissions in diesel engines. Accordingly, there is a need to improve the accuracy of NO<sub>x</sub> predictions by testing and incorporating other parameters concerning the thermal management of SCR system.

#### **4. CONCLUSIONS**

An empirical-based methodology that integrated vehicle activity and on-road emissions for DPV to predict emissions was suggested. For this purpose, on-road emissions and engine activity data were collected from four diesel vehicles, considering different driving conditions. Then, the driving style was characterized by acceleration-based parameters to validate PEMS trips and to explore their impacts on emissions. Finally, the concordance and correlation between IOV-based predictors of engine load and VSP was explored.

The analysis results show both the RPA and MPA allowed a good differentiation with respect to route trips. It was found that measured CO<sub>2</sub> emissions were inflated up to 105% when compared to the regulated level while measured NO<sub>x</sub> emissions were 3-4 times higher on average than standard emission. IOV-based predictors of engine load, in particular  $P_{MAP \times RPM}$ , were closely related with EOVB-based predictors as VSP. While for negative VSP values they were relatively constant (but varied among testing vehicles), at positive values  $P_{MAP \times RPM}$  showed good fit ( $R^2$  between 0.80 and 0.89, depending on the vehicle) using power regression analysis. These IOVs were as good as EOVB-based in predicting CO<sub>2</sub> emission rates ( $R^2$

ranged from 0.46 to 0.74, depending on the vehicle), but were worse in predicting NO<sub>x</sub> emission for small vehicle categories ( $R^2 < 0.60$ ). This happened because the operating conditions of SCR were not considered in NO<sub>x</sub> model.

As far as high emission rates are of more concern on climate change and more relevant impacts on air quality than low emission rates, IOV-based predictors must be robust for high-emitting vehicles compared to low-emitting ones.

The advantage of using IOV-based models lies in being less costing tool compare to PEMS system. The proposed methodology is of particular interest in cases where local financial resources are limited and cannot face traffic-related environmental impacts monitoring. Since IOV-based models developed here can be implemented within the ECU in order to provide real-time data on emission rates, there is the potential to share ECU-based predictions in connected vehicles. For instance, a model can be calibrated for a specific brand and model based on vehicle-specific data or be incorporated in a traffic simulation tools to assure reliable emission and air quality analysis.

The main limitation of this paper is the small sample size of the fleet that only consisted of pre-RDE DPV. This means that the models developed are only valid for those vehicles. Also, the impacts of the after-treatment system of these vehicles that results in excess NO<sub>x</sub> emissions were not considered in emission predictive models.

Thus, future research should be extended to other diesel engines with different emission standards (from Euro 1 to Euro 5 vehicles, and from Euro 6-a to Euro 6-d vehicles), as well as gasoline passenger vehicles, hybrid electric vehicles and vans. Further improvement of IOV-based models of particulate matter emissions, and incorporation of other IOVs such as IAT, catalytic temperature, exhaust flow and exhaust temperature are required to capture faithfully NO<sub>x</sub> emissions in DPV.

## **ACKNOWLEDGEMENTS**

The authors acknowledge the financial support of the following projects: TEMA – CENTRO 01-0145-FEDER-022083; Strategic Project UID/EMS/00481/2019 (FCT-Portuguese Science and Technology Foundation); MobiWise (P2020 SAICTPAC/0011/2015), co-funded by COMPETE2020, Portugal2020 - Operational Program for Competitiveness and Internationalization (POCI), European Union's ERDF (European Regional Development Fund), and FCT; @CRUiSE project (PTDC/EMS-TRA/0383/2014), funded within Project 9471 – Reforçar a Investigação, o Desenvolvimento Tecnológico e a Inovação and supported by European Community Fund FEDER; CISMOB (PGI01611, funded by Interreg Europe Programme); DICA-VE (POCI-01-0145-FEDER-029463), Driving2Driverless (POCI-01-0145-FEDER-031923) and inFLOWence (POCI-01-0145-FEDER-029679) projects funded by FEDER through COMPETE2020, and by national funds (OE), through FCT/MCTES.

## **REFERENCES**

- 3DATX, 2018. <http://www.3datx.com/>, 3-dimensional data analysis (3DATX) Corporation.
- ACAP, 2017. Estatísticas do Setor Automóvel em 2017 [In Portuguese], Automobile Association of Portugal.
- ACEA, 2019. Economic and Market Report EU Automotive Industry Full - year 2018, European Automobile Manufacturers' Association, Brussels, Belgium, Available from [https://www.acea.be/uploads/statistic\\_documents/Economic\\_and\\_Market\\_Report\\_full-year\\_2018.pdf](https://www.acea.be/uploads/statistic_documents/Economic_and_Market_Report_full-year_2018.pdf).

- Ahari, H., Smith, M., Zammit, M., Price, K., Jacques, J., Pauly, T., Wang, L., 2015. Impact of SCR Integration on N<sub>2</sub>O Emissions in Diesel Application. SAE International.
- Asprion, J., Chinellato, O., Guzzella, L., 2013. Optimisation-oriented modelling of the NO<sub>x</sub> emissions of a Diesel engine. *Energy Conversion and Management* 75, 61-73.
- Bai, S., Chen, G., Sun, Q., Wang, G., Li, G.-x., 2017. Influence of active control strategies on exhaust thermal management for diesel particulate filter active regeneration. *Applied Thermal Engineering* 119, 297-303.
- Bai, S., Han, J., Liu, M., Qin, S., Wang, G., Li, G.-x., 2018. Experimental investigation of exhaust thermal management on NO<sub>x</sub> emissions of heavy-duty diesel engine under the world Harmonized transient cycle (WHTC). *Applied Thermal Engineering* 142, 421-432.
- Charles Fayette, T., 1985. Combustion in Diesel Engines, *Internal Combustion Engine in Theory and Practice: Combustion, Fuels, Materials, Design*. MITP, p. 1.
- Chelsea Baldino, Uwe Tietge, Rachel Muncrief, Yoann Bernard, Mock, P., 2017. Road Tests: Comparative Overview of real-world versus type approval NO<sub>x</sub> and CO<sub>2</sub> Emissions from Diesel Cars in Europe., International Council on Clean Transportation: White Paper, Available at: [https://www.theicct.org/sites/default/files/publications/ICCT\\_RoadTested\\_201709.pdf](https://www.theicct.org/sites/default/files/publications/ICCT_RoadTested_201709.pdf), p. 38.
- Cho, C.P., Pyo, Y.D., Jang, J.Y., Kim, G.C., Shin, Y.J., 2017. NO<sub>x</sub> reduction and N<sub>2</sub>O emissions in a diesel engine exhaust using Fe-zeolite and vanadium based SCR catalysts. *Applied Thermal Engineering* 110, 18-24.
- Commission Regulation (EC) No 692/2008, 2008. Of 18 July 2008 implementing and amending Regulation (EC) No 715/2007 of the European Parliament and of the Council on type-approval of motor vehicles with respect to emissions from light passenger and commercial vehicles (Euro 5

and Euro 6) and on access to vehicle repair and maintenance information. *Official Journal of the European Union*, 1136.

d'Ambrosio, S., Finesso, R., Fu, L., Mittica, A., Spessa, E., 2014. A control-oriented real-time semi-empirical model for the prediction of NOx emissions in diesel engines. *Applied Energy* 130, 265-279.

Degraeuwe, B., Weiss, M., 2017. Does the New European Driving Cycle (NEDC) really fail to capture the NOX emissions of diesel cars in Europe? *Environmental Pollution* 222, 234-241.

Delavarrafiee, M., Frey, H.C., 2018. Real-world fuel use and gaseous emission rates for flex fuel vehicles operated on E85 versus gasoline. *Journal of the Air & Waste Management Association* 68(3), 235-254.

Desantes, J.M., López, J.J., Redón, P., Arrégle, J., 2012. Evaluation of the Thermal NO formation mechanism under low-temperature diesel combustion conditions. *International Journal of Engine Research* 13(6), 531-539.

EC, 1999. Regulation (EEC) No 4064/89 merger procedure,, *EC – European Commission, Available from [http://ec.europa.eu/competition/mergers/cases/decisions/m1406\\_en.pdf](http://ec.europa.eu/competition/mergers/cases/decisions/m1406_en.pdf)*.

EC, 2016. Commission Regulation (EU) 2016/646 of 20 April 2016 amending Regulation (EC) No 692/2008 as regards emissions from light passenger and commercial vehicles (Euro 6). *Official Journal of the European Union*, 22.

EC, 2017. Commission Regulation (EU) 2017/1151 of 1 June 2017 supplementing Regulation (EC) No. 715/2007 of the European Parliament and of the Council on type-approval of motor vehicles with respect to emissions from light passenger and commercial vehicles (Euro 5 and Euro 6) and on access to vehicle repair and maintenance information, amending Directive 2007/46/EC of the

European Parliament and of the Council, Commission Regulation (EC) No. 692/2008 and Commission Regulation (EU) No. 1230/2012 and repealing Commission Regulation (EC) No. 692/2008. *Official Journal of the European Union*, 643.

EEA, 2016. Explaining road transport emissions - A non-technical guide, European Environmental Agency, Copenhagen, Denmark, Available from <https://www.eea.europa.eu/publications/explaining-road-transport-emissions>.

EEA, 2018a. Air quality in Europe — 2018 report.

EEA, 2018b. EMEP/EEA air pollutant emission inventory guidebook 2016 – 1.A.3.b.i, 1.A.3.b.ii, 1.A.3.b.iii, 1.A.3.b.iv Passenger cars, light commercial trucks, heavy - duty vehicles including buses and motor cycles *EEA – European Environment Agency, Available from <https://www.eea.europa.eu/publications/emep-eea-guidebook-2016/part-b-sectoral-guidance-chapters/1-energy/1-a-combustion/1-a-3-b-i/view>*.

EEA, 2019a. Average carbon dioxide emissions from new passenger cars, Available from: [https://www.eea.europa.eu/data-and-maps/daviz/average-emissions-for-new-cars-5#tab-googlechartid\\_chart\\_11](https://www.eea.europa.eu/data-and-maps/daviz/average-emissions-for-new-cars-5#tab-googlechartid_chart_11).

EEA, 2019b. Final energy consumption by sector and fuel, March, 2019 [cited March 2019], European Environmental Agency, Copenhagen, Denmark, Available from <https://www.eea.europa.eu/data-and-maps/indicators/final-energy-consumption-by-sector-9/assessment-4>.

Engineering ToolBox, 2019. Density of fuel oils as function of temperature, Available from [https://www.engineeringtoolbox.com/fuel-oil-density-temperature-gravity-volume-correction-ASTM-D1250-d\\_1942.html](https://www.engineeringtoolbox.com/fuel-oil-density-temperature-gravity-volume-correction-ASTM-D1250-d_1942.html).

- EPA, 2018. <https://www.govinfo.gov/content/pkg/CFR-2012-title40-vol19/xml/CFR-2012-title40-vol19-sec86-144-94.xml>, In: emissions., S.-.-C.e. (Ed.), Title 40 - Protection of Environment. CHAPTER I - ENVIRONMENTAL PROTECTION AGENCY (CONTINUED). SUBCHAPTER C - AIR PROGRAMS (CONTINUED). PART 86 - CONTROL OF EMISSIONS FROM NEW AND IN-USE HIGHWAY VEHICLES AND ENGINES. Subpart B - Emission Regulations for 1977 and Later Model Year New Light-Duty Vehicles and New Light-Duty Trucks and New Otto-Cycle Complete Heavy-Duty Vehicles; Test Procedures.
- ERSI, 2016. *About ArcGIS / Mapping & Analytics Platform*. ERSI - Environmental System Research Institute, Retrieved from: <https://www.esri.com/en-us/arcgis/about-arcgis/overview>.
- EU, 2017. Energy, transport and environment indicators - 2017 edition, , *Publications Office of the European Union, Luxembourg, Luxembourg, Available from <https://ec.europa.eu/eurostat/documents/3217494/8435375/KS-DK-17-001-EN-N.pdf/18d1ecfd-acd8-4390-ade6-e1f858d746da>*.
- Farrance, I., Frenkel, R., 2012. Uncertainty of Measurement: A Review of the Rules for Calculating Uncertainty Components through Functional Relationships. *Clin Biochem Rev* 33(2), 49-75.
- Fontaras, G., Zacharof, N.-G., Ciuffo, B., 2017. Fuel consumption and CO2 emissions from passenger cars in Europe – Laboratory versus real-world emissions. *Progress in Energy and Combustion Science* 60, 97-131.
- Frey, H.C., Zhang, K., Roupail, N.M., 2008. Fuel Use and Emissions Comparisons for Alternative Routes, Time of Day, Road Grade, and Vehicles Based on In-Use Measurements. *Environmental Science & Technology* 42(7), 2483-2489.



- Gallus, J., Kirchner, U., Vogt, R., Benter, T., 2017. Impact of driving style and road grade on gaseous exhaust emissions of passenger vehicles measured by a Portable Emission Measurement System (PEMS). *Transportation Research Part D: Transport and Environment* 52, 215-226.
- Giechaskiel, B., Clairotte, M., Valverde-Morales, V., Bonnel, P., Kregar, Z., Franco, V., Dilara, P., 2018. Framework for the assessment of PEMS (Portable Emissions Measurement Systems) uncertainty. *Environmental Research* 166, 251-260.
- Giechaskiel, B., Maricq, M., Ntziachristos, L., Dardiotis, C., Wang, X., Axmann, H., Bergmann, A., Schindler, W., 2014. Review of motor vehicle particulate emissions sampling and measurement: From smoke and filter mass to particle number. *Journal of Aerosol Science* 67, 48-86.
- Guardiola, C., Martín, J., Pla, B., Bares, P., 2017. Cycle by cycle NO<sub>x</sub> model for diesel engine control. *Applied Thermal Engineering* 110, 1011-1020.
- Guardiola, C., Pla, B., Blanco-Rodriguez, D., Calendini, P.O., 2014. ECU-oriented models for NO<sub>x</sub> prediction. Part 1: a mean value engine model for NO<sub>x</sub> prediction. *Proceedings of the Institution of Mechanical Engineers, Part D: Journal of Automobile Engineering* 229(8), 992-1015.
- Holmén, B.A., Sentoff, K.M., 2015. Hybrid-Electric Passenger Car Carbon Dioxide and Fuel Consumption Benefits Based on Real-World Driving. *Environmental Science & Technology* 49(16), 10199-10208.
- Hooftman, N., Messagie, M., Van Mierlo, J., Coosemans, T., 2018. A review of the European passenger car regulations – Real driving emissions vs local air quality. *Renewable and Sustainable Energy Reviews* 86, 1-21.

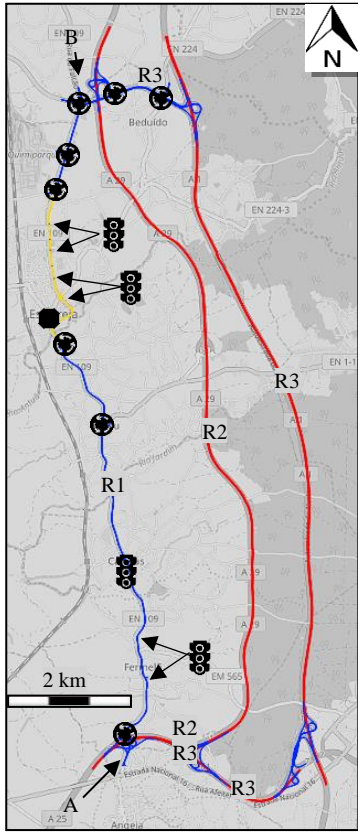
- Hu, J., Frey, H.C., Washburn, S.S., 2016. Comparison of Vehicle-Specific Fuel Use and Emissions Models Based on Externally and Internally Observable Activity Data. *Transportation Research Record* 2570(1), 30-38.
- Hu, X., Shi, Q., Zhang, H., Wang, P., Zhan, S., Li, Y., 2017. NH<sub>3</sub>-SCR performance improvement over Mo modified Mo(x)-MnO<sub>x</sub> nanorods at low temperatures. *Catalysis Today* 297, 17-26.
- IMT, 2019. *Relatório de Tráfego na Rede Nacional de Auto-Estradas [In Portuguese]*, Portuguese Institute for Mobility and Transport. Portuguese Institute for Mobility and Transport, Retrieved from: <http://www.imt-ip.pt/sites/IMTT/Portugues/InfraestruturasRodoviaras/RedeRodoviaria/Relatrios/Relat%C3%B3rio%20de%20Tr%C3%A1fego%20-%204%C2%BA%20Trimestre%20de%202018.pdf>, April 8, 2019.
- Jiménez-Palacios, J.L., 1999. Understanding and quantifying motor vehicle emissions with vehicle specific power and TILDAS remote sensing. PhD dissertation. Massachusetts Institute of Technology, Cambridge.
- Johnson, T., 2016. Vehicular Emissions in Review. SAE International, pp. 1258-1275.
- Kwon, S., Park, Y., Park, J., Kim, J., Choi, K.-H., Cha, J.-S., 2017. Characteristics of on-road NO<sub>x</sub> emissions from Euro 6 light-duty diesel vehicles using a portable emissions measurement system. *Science of The Total Environment* 576, 70-77.
- Leland, A., Stanard, A., 2018. Light Duty PEMS Validations/Chassis Dynamometer Correlation, Coordinating Research Council (CRC), Prepared by the Eastern Research Group, Inc, Report: ERG No. 4043.00.001.001 Project E-122, p. 177.

- Liu, H., Gegov, A., Cocea, M., 2017. Unified Framework for Control of Machine Learning Tasks Towards Effective and Efficient Processing of Big Data, In: Pedrycz, W., Chen, S.-M. (Eds.), *Data Science and Big Data: An Environment of Computational Intelligence*. Springer International Publishing, Cham, pp. 123-140.
- Liu, Y., Lee, J.-M., 2018. Conventional and New Materials for SCR NO<sub>x</sub> Catalytic Reduction. *ChemCatChem* 10, 1499-1511.
- Luján, J.M., Bermúdez, V., Dolz, V., Monsalve-Serrano, J., 2018. An assessment of the real-world driving gaseous emissions from a Euro 6 light-duty diesel vehicle using a portable emissions measurement system (PEMS). *Atmospheric Environment* 174, 112-121.
- Mahesh, S., Ramadurai, G., Shiva Nagendra, S.M., 2018. Real-world emissions of gaseous pollutants from diesel passenger cars using portable emission measurement systems. *Sustainable Cities and Society* 41, 104-113.
- Newman, M.C., 1993. Regression analysis of log-transformed data: Statistical bias and its correction. *Environmental Toxicology and Chemistry* 12(6), 1129-1133.
- Ntziachristos, L., Papadimitriou, G., Ligterink, N., Hausberger, S., 2016. Implications of diesel emissions control failures to emission factors and road transport NO<sub>x</sub> evolution. *Atmospheric Environment* 141, 542-551.
- O'Driscoll, R., Stettler, M.E.J., Molden, N., Oxley, T., ApSimon, H.M., 2018. Real world CO<sub>2</sub> and NO<sub>x</sub> emissions from 149 Euro 5 and 6 diesel, gasoline and hybrid passenger cars. *Science of The Total Environment* 621, 282-290.


- Sandhu, G., Frey, H., 2013a. Effects of Errors on Vehicle Emission Rates from Portable Emissions Measurement Systems. *Transportation Research Record: Journal of the Transportation Research Board* 2340, 10-19.
- Sandhu, G.S., Frey, H.C., 2013b. Effects of Errors on Vehicle Emission Rates from Portable Emissions Measurement Systems. *Transportation Research Record* 2340(1), 10-19.
- Seneque, M., Can, F., Duprez, D., Courtois, X., 2015. Use of a  $\mu$ -Scale Synthetic Gas Bench for Direct Comparison of Urea-SCR and NH<sub>3</sub>-SCR Reactions over an Oxide Based Powdered Catalyst. *Catalysts* 5(3), 1535-1553.
- Sileghem, L., Bosteels, D., May, J., Favre, C., Verhelst, S., 2014. Analysis of vehicle emission measurements on the new WLTC, the NEDC and the CADC. *Transportation Research Part D: Transport and Environment* 32, 70-85.
- USEPA, 2002. Methodology for developing modal emission rates for EPA's multi-scale motor vehicle & equipment emission system, Ann Arbor, MI: Prepared by North Carolina State University for US Environmental Protection Agency; 286 p. Report No.: EPA420-R-02-027.
- Weiss, M., Bonnel, P., Kühlwein, J., Provenza, A., Lambrecht, U., Alessandrini, S., Carriero, M., Colombo, R., Forni, F., Lanappe, G., Le Lijour, P., Manfredi, U., Montigny, F., Sculati, M., 2012. Will Euro 6 reduce the NO<sub>x</sub> emissions of new diesel cars? – Insights from on-road tests with Portable Emissions Measurement Systems (PEMS). *Atmospheric Environment* 62, 657-665.
- White, L., Miles, A., Boocock, C., Cooper, J.-G., Mills, S., 2018. A comparison of real driving emissions from Euro 6 diesel passenger cars with zero emission vehicles and their impact on urban air quality compliance - Report no. 8/1, Prepared for Concawe by Aeris, Available from

[https://www.acea.be/uploads/statistic\\_documents/Economic\\_and\\_Market\\_Report\\_full-year\\_2018.pdf](https://www.acea.be/uploads/statistic_documents/Economic_and_Market_Report_full-year_2018.pdf).

- Yang, Z., Ge, Y., Thomas, D., Wang, X., Su, S., Li, H., He, H., 2019. Real driving particle number (PN) emissions from China-6 compliant PFI and GDI hybrid electrical vehicles. *Atmospheric Environment* 199, 70-79.
- Yazdani Boroujeni, B., Frey, H.C., 2014. Road grade quantification based on global positioning system data obtained from real-world vehicle fuel use and emissions measurements. *Atmospheric Environment* 85, 179-186.
- Yuan, W., Frey, H.C., Wei, T., Rastogi, N., VanderGriend, S., Miller, D., Mattison, L., 2019. Comparison of real-world vehicle fuel use and tailpipe emissions for gasoline-ethanol fuel blends. *Fuel* 249, 352-364.
- Zhang, L., Hu, X., Qiu, R., Lin, J., 2019. Comparison of real-world emissions of LDGVs of different vehicle emission standards on both mountainous and level roads in China. *Transportation Research Part D: Transport and Environment* 69, 24-39.



**GPS Coordinates**  
**A** 40°41'13.48"N 8°33'27.25"W  
**B** 40°47'4.46"N 8°33'57.01"W

 Roundabout  
  Stop Controlled  
  Traffic Light

**FIGURE 1** Routes Aerial View. Background Map Source [Open Street Maps].

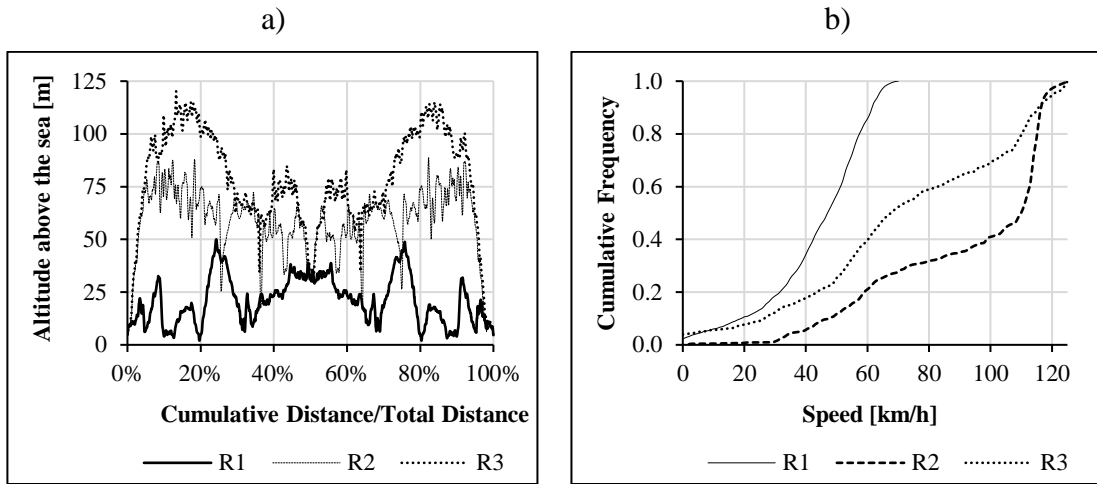


**FIGURE 2** Test routes: a) altitude profiles; and b) typical speed distribution.

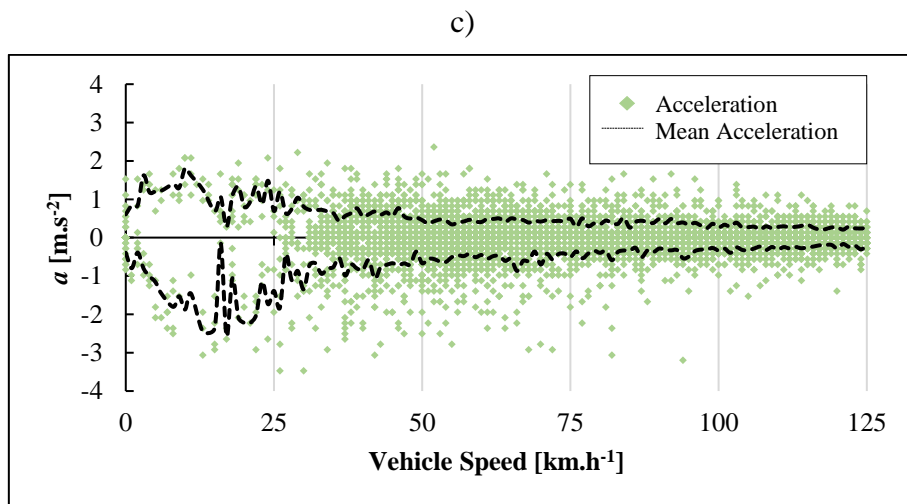
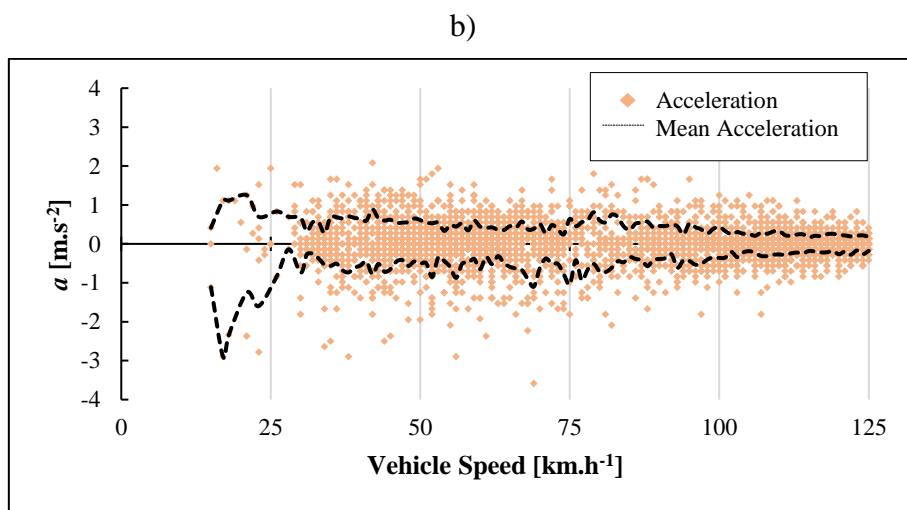
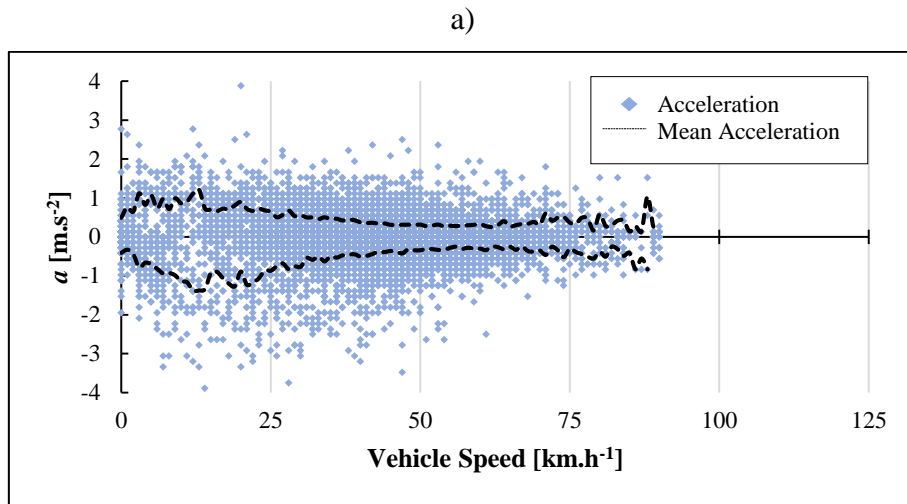


**FIGURE 3** Acceleration as a function of vehicle speed by vehicle route: a) R1; b) R2; and c) R3.



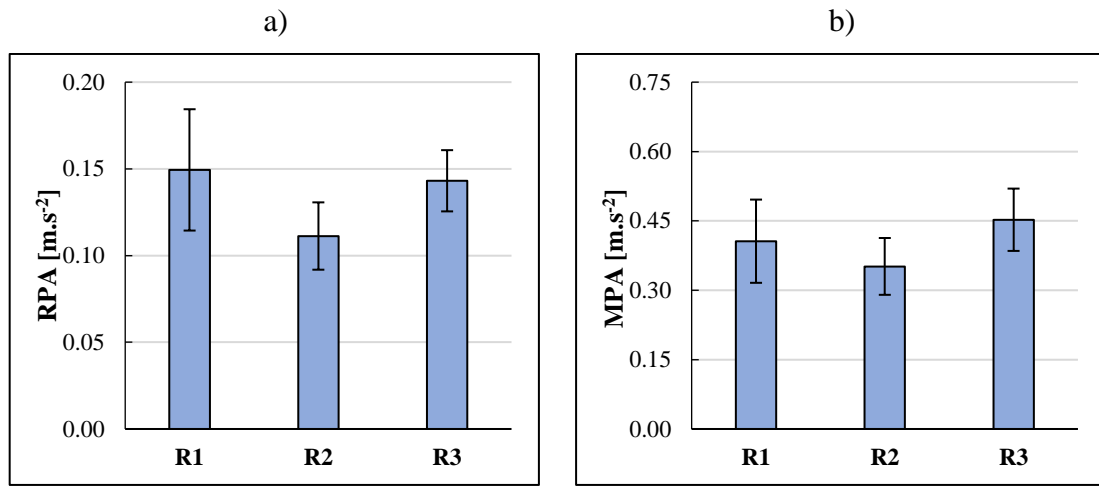


**FIGURE 4** Driving dynamics of the PEMS trips: a) RPA by route; and b) MPA by route.

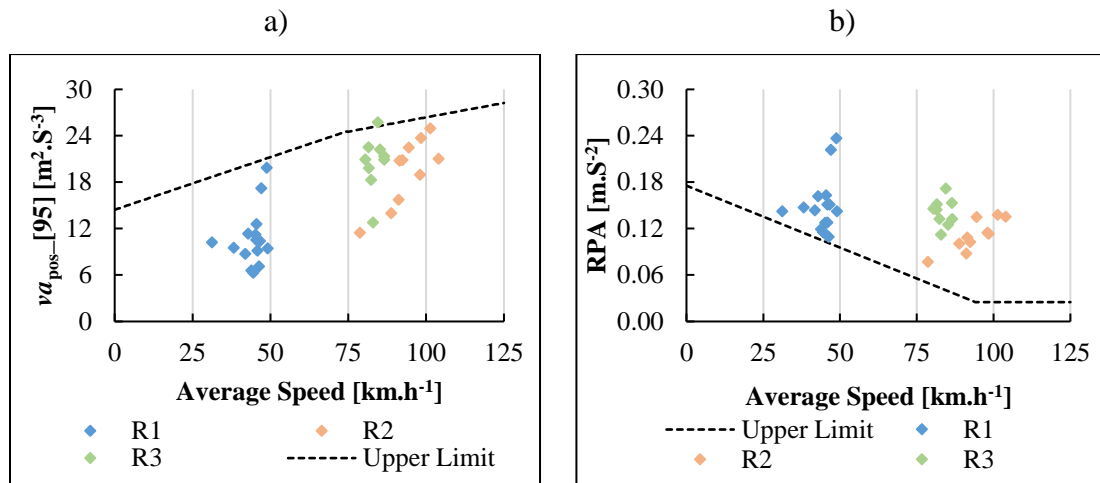
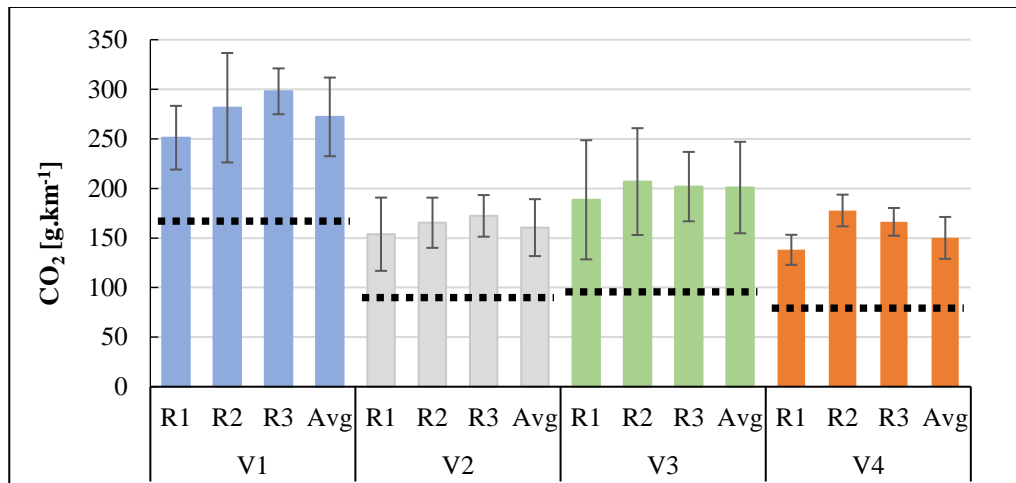
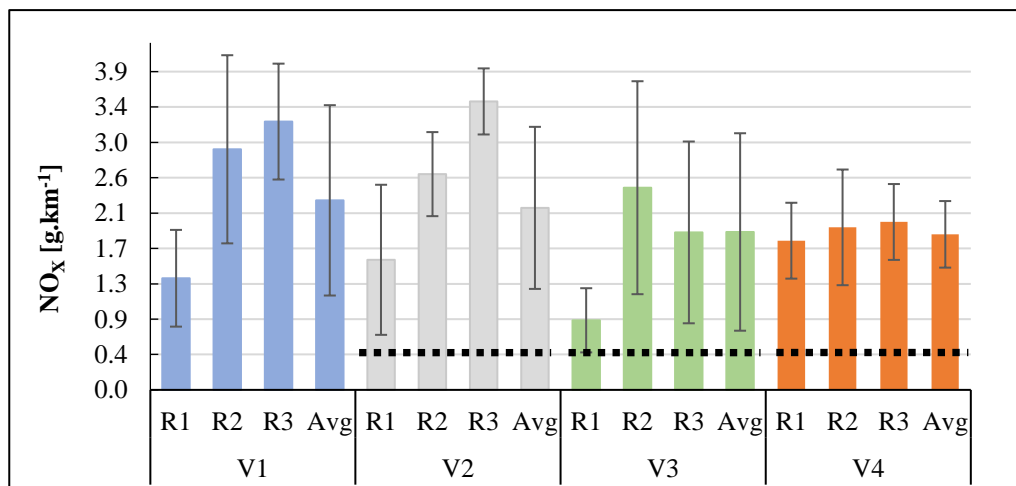


**FIGURE 5** Validation of PEMS trips: a)  $va_{pos\_95}$  by speed; and b) RPA by speed.

a)

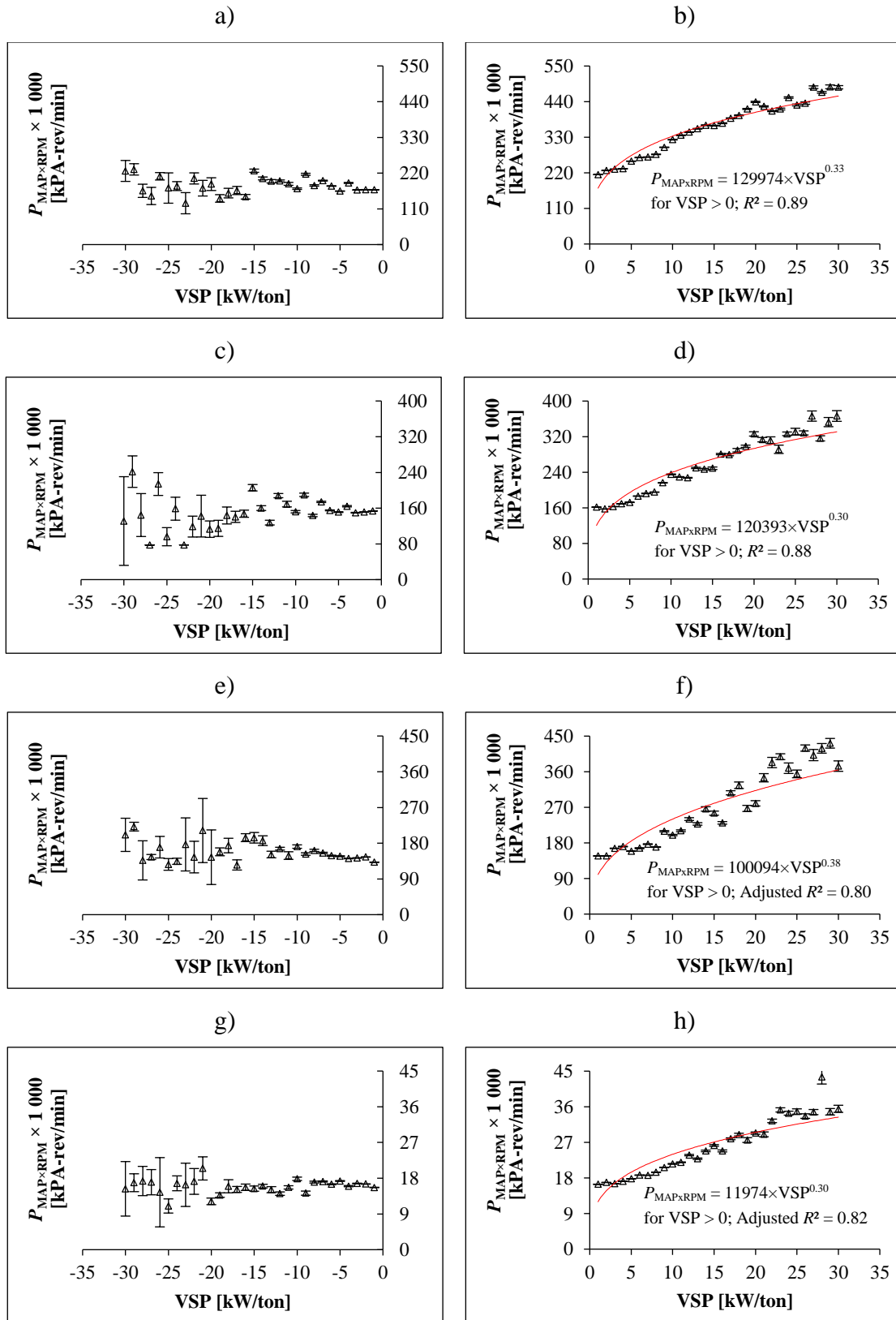


b)



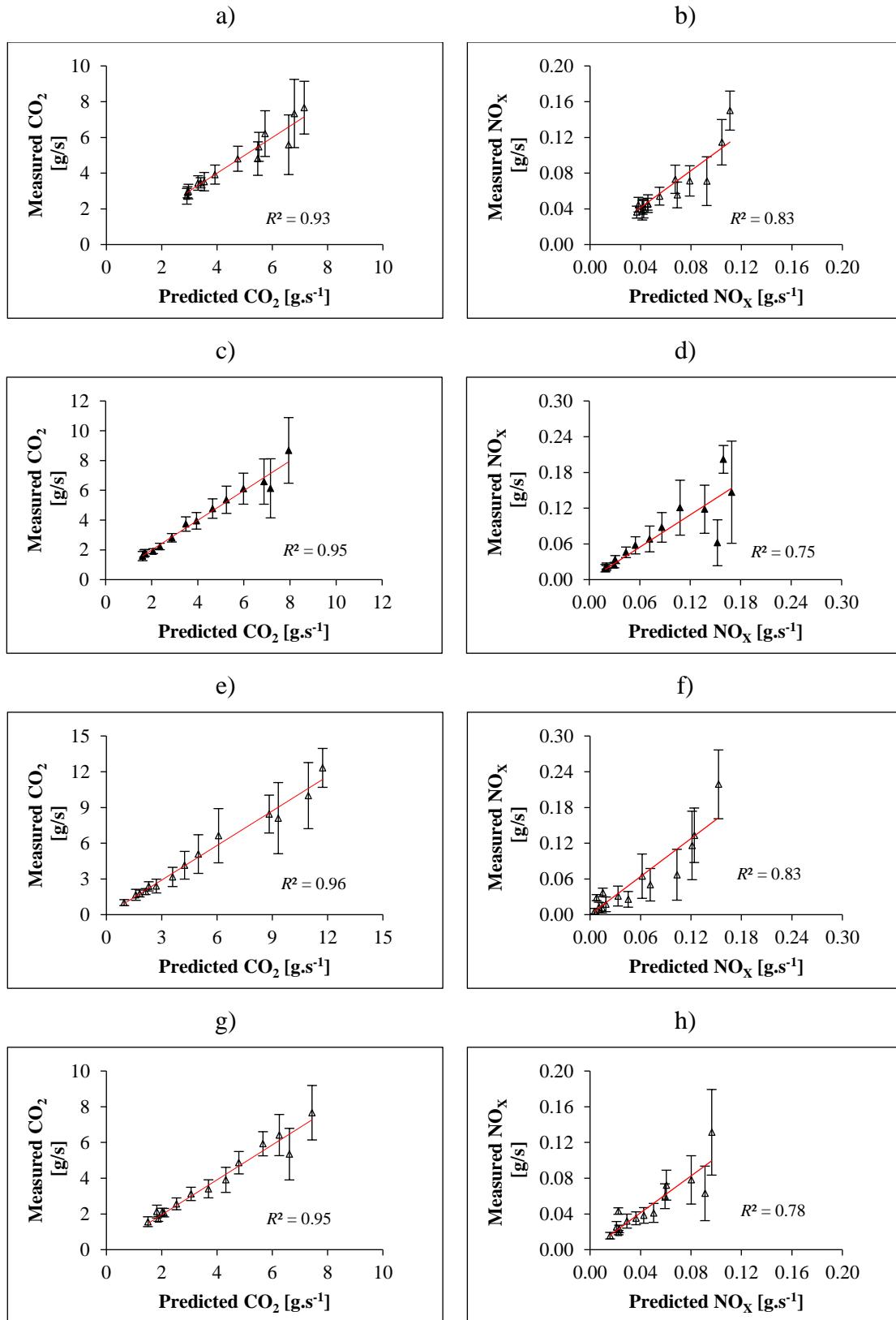
Note: Dashed lines represent vehicle-specific CO<sub>2</sub> approval and Euro 6b NO<sub>x</sub> limit. The conformity factor for NO<sub>x</sub> was 5.35 (i.e., NO<sub>x</sub> = 0.428 g.km<sup>-1</sup>), as suggested by White et al. (2018).

**FIGURE 6** Average emissions (with standard deviation values) by vehicle and route: a) CO<sub>2</sub> per unit distance; and b) NO<sub>x</sub> per unit distance.



Note: Error bars represent 95% confidence level

**FIGURE 7** Measured  $P_{MAP \times RPM}$  versus  $VSP$ , with 1-kW/ton intervals, by vehicle: a) V1 –  $VSP < 0$ ; b) V1 –  $VSP > 0$ ; c) V2 –  $VSP < 0$ ; d) V2 –  $VSP > 0$ ; e) V3 –  $VSP < 0$ ; f) V3 –  $VSP > 0$ ; g) V4 –  $VSP < 0$ ; and h) V4 –  $VSP > 0$ .



Note: Predicted CO<sub>2</sub>/NO<sub>x</sub> is the emission rates from the training set; Measured CO<sub>2</sub>/NO<sub>x</sub> is the emission rates from the testing set.

**FIGURE 8** Comparison between measured and predicted emission rates based on VSP-modal approach, by vehicle: a) V1 – CO<sub>2</sub>; b) V1 – NO<sub>x</sub>; c) V2 – CO<sub>2</sub>; d) V2– NO<sub>x</sub>; e) V3 – CO<sub>2</sub>; f) V3 – NO<sub>x</sub>; g) V4 – CO<sub>2</sub>; and h) V4 – NO<sub>x</sub>.

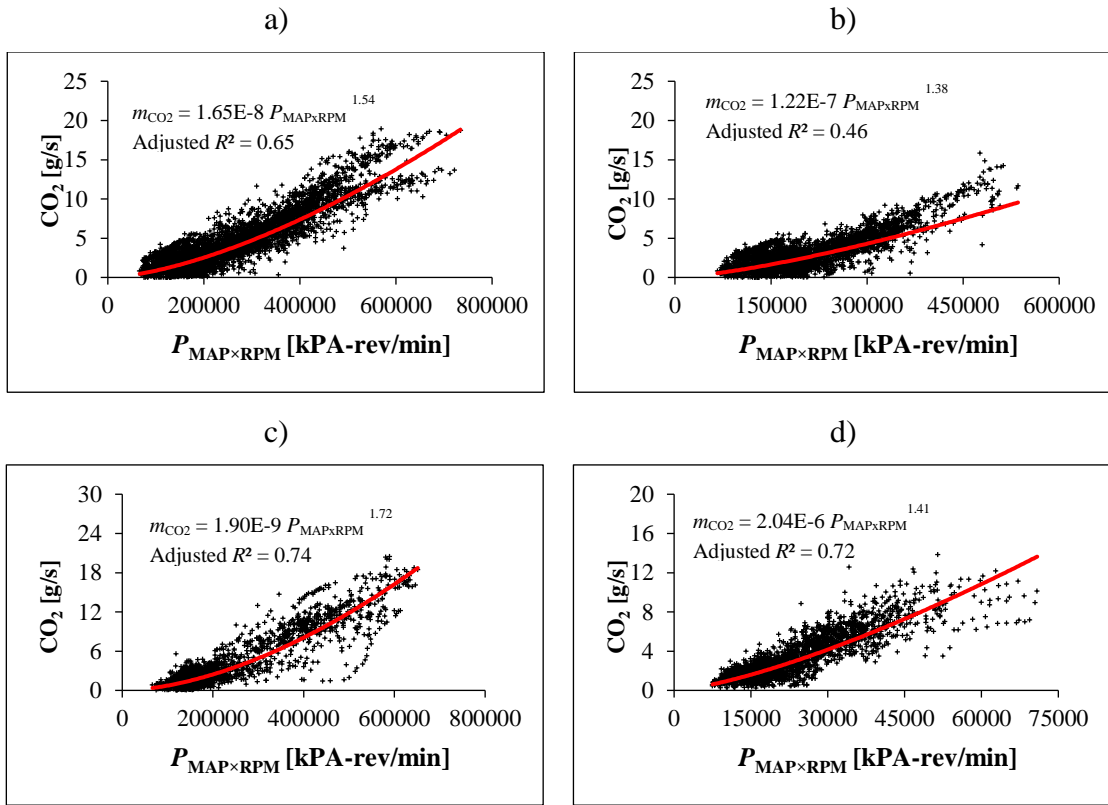


**FIGURE 9** CO<sub>2</sub> emission rates versus IOVs, by vehicle: a) V1 b) V2; c) V3; and d) V4.

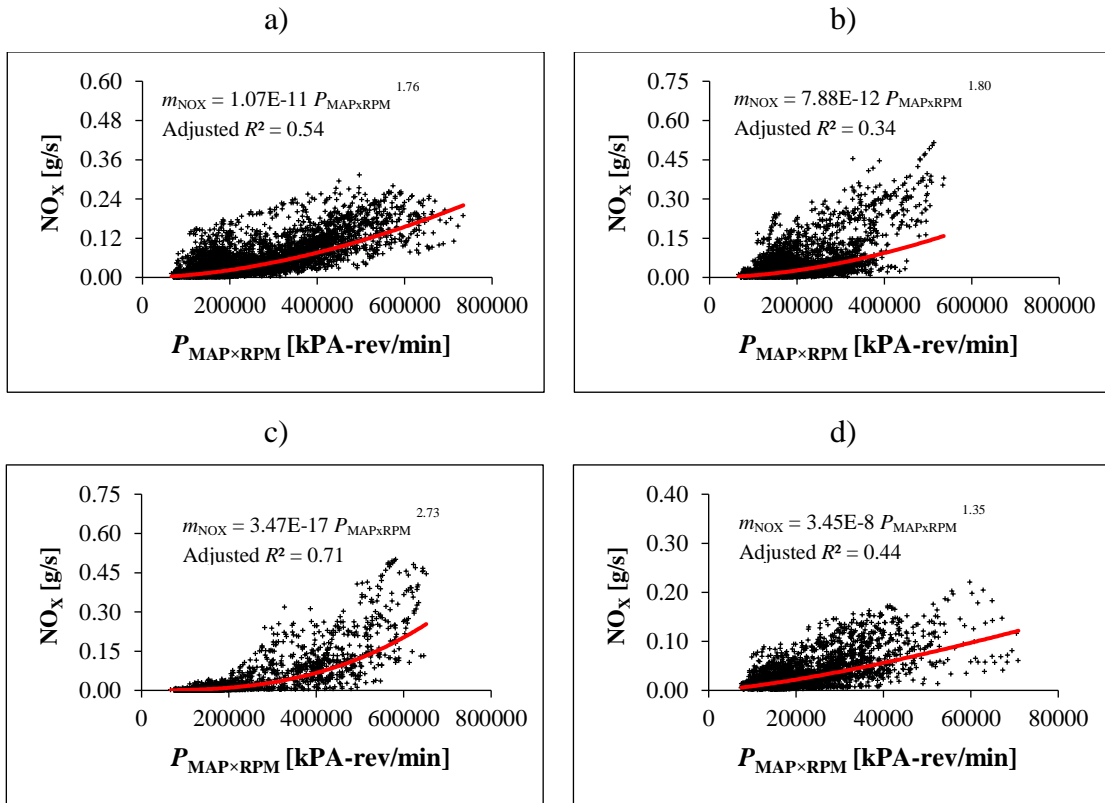
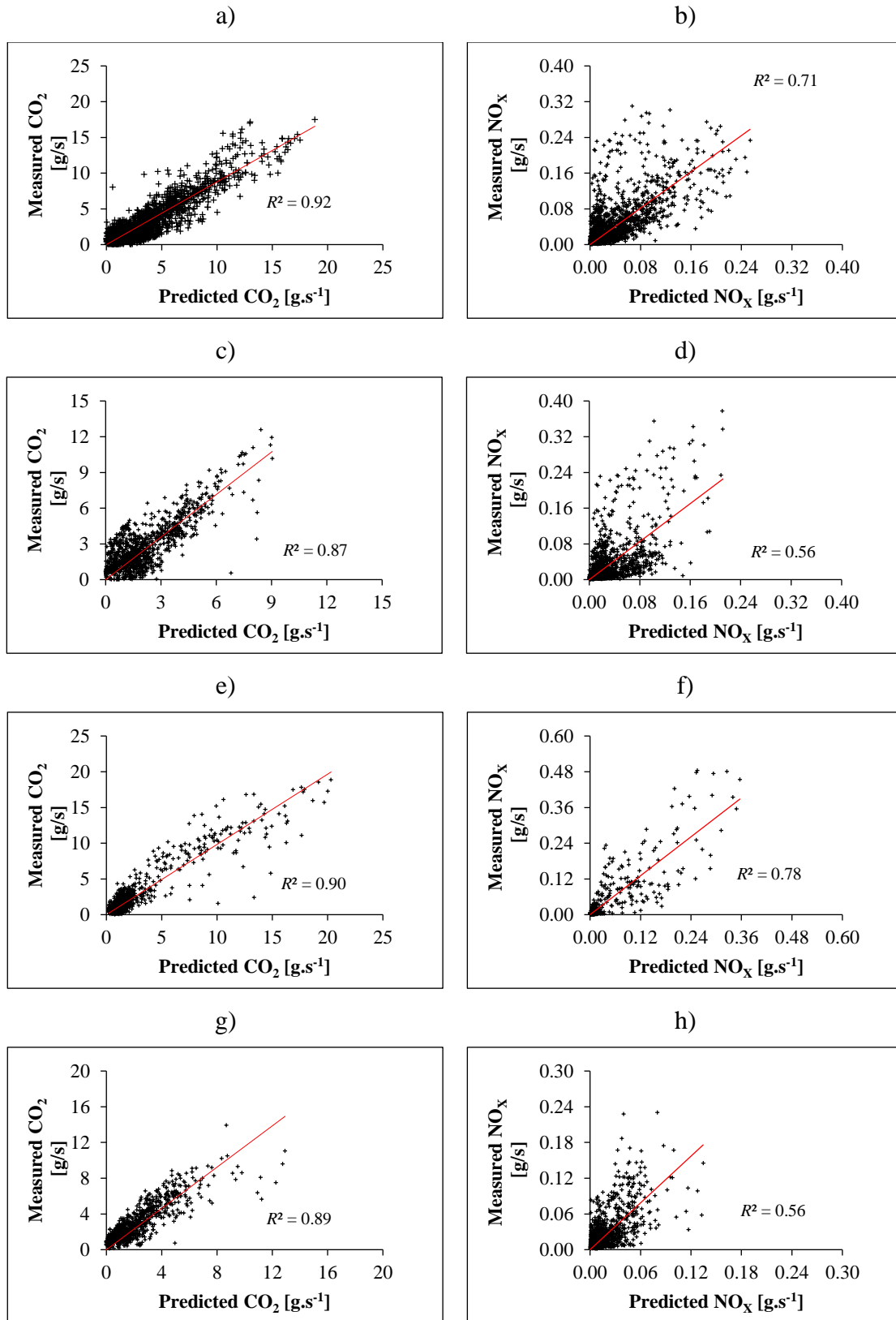


**FIGURE 10** NO<sub>x</sub> emission rates versus IOVs, by vehicle: a) V1 b) V2; c) V3; and d) V4.



Note: Predicted CO<sub>2</sub>/NO<sub>x</sub> is the emission rates from the training set; Measured CO<sub>2</sub>/NO<sub>x</sub> is the emission rates from the testing set.

**FIGURE 11** Comparison between measured and predicted emission rates based on IOV-based model, by vehicle: a) V1 – CO<sub>2</sub>; b) V1 – NO<sub>x</sub>; c) V2 – CO<sub>2</sub>; d) V2 – NO<sub>x</sub>; e) V3 – CO<sub>2</sub>; f) V3 – NO<sub>x</sub>; g) V4 – CO<sub>2</sub>; and h) V4 – NO<sub>x</sub>.



**TABLE 1** Key studies on emission measurements of DPV, LPV and HEV.

Reference	Test Fleet	Variables	Major findings	Observations
<b>Weiss et al. (2012)</b>	One DPV (Euro 6) 4 DPV (Euro 5) 2 DPV (Euro 4)	Total Hydrocarbons (THC), CO, NO/ NO <sub>x</sub> CO <sub>2</sub>	On-road NO <sub>x</sub> exceeded their emissions standards standard by $260 \pm 130\%$ ; On-road CO <sub>2</sub> deviated by $8 \pm 13\%$ from the NEDC values	No method to predict emissions rates based on EOVs or IOVs
<b>Boroujeni et al. (2014)</b>	3 SUVs, 2 Pick-up trucks 7 Sedans	Fuel Use, NO <sub>x</sub> , HC, CO, Road Grade; Speed, RPM, MAP, Mass air flow (MAF)	The net effect of grades along a route was found to be significant in NO <sub>x</sub> and CO emissions	No method to predict emissions rates based on IOVs
<b>Holmén and Sentoff (2015)</b>	One HEV One GPV	Fuel Use, CO <sub>2</sub> RPM, MAF, Speed,	HEV CO <sub>2</sub> emission benefit factors, frequency of electric-drive-only operation, ranged from 1.4 to 4.5 (depending on trip section)	CO <sub>2</sub> and fuel use predictions based on EOVs (VSP)
<b>Hu et al. (2016)</b>	6 GPVs 4 Gasoline Passenger Trucks	Fuel Use, NO <sub>x</sub> , HC, CO, GPS Data, Intake air Temperature (IAT), Speed, MAF, Mass fuel flow	IOV-based models (product of MAP and RPM) were generally better predictors of emission rates than VSP-based model	Goodness-of-fit varied among test vehicles;
<b>Chelsea et al. (2017)</b>	541 DPVs (Euro 5-6)	CO <sub>2</sub> , NO <sub>x</sub>	Higher real-world emissions compared to standard laboratory tests: NO <sub>x</sub> emissions' conformity factors exceeded 1 to 11 times (depending on the vehicle); CO <sub>2</sub> gap was approximately 30%	No method to predict emissions rates based on EOVs or IOVs
<b>Galus et al. (2017)</b>	2 DPVs (Euro 5-6)	CO <sub>2</sub> , NO <sub>x</sub> , Speed	For a road grade change from 0% to 5%, CO <sub>2</sub> and NO <sub>x</sub> emissions increased more than 65%; CO <sub>2</sub> and NO <sub>x</sub> emissions increased up to 40% and 255%, respectively, in trips with larger RPA, MPA and $a \times v$	No method to predict emissions rates based on EOVs or IOVs
<b>Kwon et al. (2017)</b>	6 DPVs (Euro 6)	CO <sub>2</sub> , NO <sub>x</sub> Speed	On-road NO <sub>x</sub> emissions highly effect on the driving route and meteorological conditions	No method to predict emissions rates based on EOVs or IOVs
<b>Luján et al. (2018)</b>	One DPV (Euro 6)	CO, CO <sub>2</sub> , NO/NO <sub>x</sub> , NO <sub>2</sub> , THC Exhaust flow rate	Differences in analytical methods proposed by RDE on emissions conformity factor calculations (10% to 45% depending on the pollutant and the trip section considered)	No method to predict emissions rates based on EOVs or IOVs
<b>O'Driscoll et al. (2018)</b>	149 Vehicles: GPVs, DPVs and 2 HEVs (Euro 5-6)	CO <sub>2</sub> , NO <sub>x</sub> , Hydrocarbons (HC), GPS Data	DPVs had lower CO <sub>2</sub> emissions than GPVs (11% to 40%); DPVs NO <sub>x</sub> were 300% to 450% higher than the emission standard	No method to predict emissions rates based on EOVs or IOVs
<b>Yang et al. (2019)</b>	2 HEV (China 6)	PN, Speed, RPM Intake Mass Flow Rates; Exhaust Temperature; Throttle Position	Both cars failed the Euro-6 PN limit (34% and 99%); IOVs were plotted against PN concentrations in different trip sections	No method to predict emissions rates based on EOVs or IOVs
<b>Yuan et al. (2019)</b>	3 Tier 3; 2 Tier 2 (one flexible-fuel vehicle -FFV and 4 non-FFVs)	CO <sub>2</sub> , CO, HC, NO <sub>x</sub> and particulate matter (PM)	Each car was measured with neat gasoline (E0), 10% ethanol by volume (E10) "regular" (E10R) and "premium" (E10P), and 27% ethanol by volume (E27). E27 had low CO emission rates compared to the other three fuels. No significant difference was found in NO <sub>x</sub> for E27 versus the other fuels.	No method to predict emissions rates based on EOVs or IOVs
<b>Zhang et al. (2019)</b>	6 GPV (China 3 to 5)	CO, HC, CO <sub>2</sub> , NO <sub>x</sub> GPS Data; Speed	Newer vehicles produced much lower CO ( $\square 67\%$ ) and NO <sub>x</sub> ( $\square 31\%$ ) emissions than older vehicles on hilling roads	No method to predict emissions rates based on IOVs

**TABLE 2** Technical specifications of the test vehicles.

<b>Vehicle ID</b>	<b>Emission Standard</b>	<b>Vehicle Category<sup>1</sup></b>	<b>Model Year</b>	<b>Engine Size (L)</b>	<b>Odometer reading at test start (km)</b>
<b>V1</b>	Euro 4	M	June 2006	1.8	□180 000
<b>V2</b>	Euro 6b	B	January 2017	1.2	□32 000
<b>V3</b>	Euro 6b	C	July2017	1.6	□23 000
<b>V4</b>	Euro 6b	B	March 2018	1.5	□25 000

<sup>1</sup> Categorization of vehicles is based on EC (1999): B – Small Cars; C – Medium Cars; M – Multi-purpose cars

**TABLE 3** Measurements Principles and Sample Condition of the selected PEMS.

<b>Measurement</b>	<b>3DATX</b>
CO/HC	Not Applicable
NO <sub>x</sub>	NO (ppm) and NO <sub>2</sub> (ppm) separately – Electrochemical
CO <sub>2</sub>	In volume fraction ( $X_{CO_2}$ ) by non-dispersive infrared
Exhaust Flow	None
Gaseous Sample Conditioning	Chiller captures condensed water
PM Measurement	No mass estimation

**TABLE 4** Summary of ambient and activity real-world data for selected vehicle types operated on R1, R2 and R3 routes (both directions of travelling).

Parameter	Vehicle	R1	R2	R3
Driving Time (minutes)	V1	117	72	75
	V2	98	45	53
	V3	101	42	32
	V4	107	32	36
Average OBD Speed (km.h <sup>-1</sup> )	V1	46	95	82
	V2	43	88	79
	V3	38	100	86
	V4	46	91	83
Min to max MAF (g.s <sup>-1</sup> )	V1	4 – 119	4 – 113	4 – 118
	V2	5 – 40	7 – 53	6 – 49
	V3	4 – 56	7 – 83	5 – 81
	V4	4 – 68	5 – 77	6 – 78
Min to max MAP (kPA)	V1	95 – 255	98 – 255	97 – 255
	V2	71 – 196	83 – 228	83 – 237
	V3	99 – 196	101 – 235	100 – 232
	V4	10 – 25	10 – 24	10 – 24
Min to max RPM (rpm)	V1	770 – 3 140	860 – 2 900	820 – 3 300
	V2	720 – 2 330	805 – 2 520	770 – 2 420
	V3	650 – 2 195	740 – 2 900	744 – 2 850
	V4	690 – 2 820	850 – 2 890	650 – 2 950
Min to max IAT (°C)	V1	13 – 21	14 – 18	13 – 17
	V2	16 – 31	15 – 19	14 – 18
	V3	15 – 38	16 – 31	18 – 30
	V4	20 – 28	19 – 27	20 – 29
Min to max T (°C)	V1	14 – 18	14 – 18	14 – 18
	V2	13 – 17	13 – 17	13 – 17
	V3	12 – 15	12 – 15	12 – 15
	V4	13 – 16	13 – 16	13 – 16
Min to max H (%)	V1	57 – 69	55 – 68	55 – 63
	V2	40 – 65	66 – 68	70 – 71
	V3	78 – 83	71 – 84	72 – 82
	V4	69 – 75	66 – 70	70 – 72
Min to max X <sub>CO2</sub> (%)	V1	1 – 15	1 – 14	2 – 16
	V2	1 – 19	1 – 18	1 – 18
	V3	1 – 15	1 – 17	2 – 17
	V4	1 – 15	2 – 18	1 – 17
Min to max NO (ppm)	V1	102 – 1 727	120 – 2 220	230 – 3 750
	V2	37 – 9 715	111 – 7 690	147 – 6 990
	V3	59 – 1 530	61 – 4 300	60 – 3 750
	V4	100 – 5 500	155 – 3 350	101 – 4 580
Min to max NO <sub>2</sub> (ppm)	V1	6 – 58	5 – 58	5 – 63
	V2	1 – 94	2 – 167	4 – 120
	V3	1 – 48	1 – 48	1 – 40
	V4	2 – 63	4 – 70	3 – 77

**TABLE 5** Summary of uncertainty values used in this study (EC, 2016; Giechaskiel et al., 2018).

Parameter	Requirement	Symbol	Value
OBD	MAF – Sensor Accuracy	$\epsilon_{\text{MAF}}$	10%
	FFR – Sensor Accuracy	$\epsilon_{\text{FFR}}$	10%
NO Analyzer	Analyzer Accuracy	$\epsilon_{\text{NO,acc}}$	2%
	Linearity	$\epsilon_{\text{NO,lin}}$	1%
	Span Drift	$\epsilon_{\text{NO,span}}$	2%
	Gas Accuracy	$\epsilon_{\text{NO,gas}}$	2%
NO <sub>2</sub> Analyzer	Analyzer Accuracy	$\epsilon_{\text{NO}_2,\text{acc}}$	2%
	Linearity	$\epsilon_{\text{NO}_2,\text{lin}}$	1%
	Span Drift	$\epsilon_{\text{NO}_2,\text{span}}$	2%
	Gas Accuracy	$\epsilon_{\text{NO}_2,\text{gas}}$	2%
CO <sub>2</sub> Analyzer	Analyzer Accuracy	$\epsilon_{\text{CO}_2,\text{acc}}$	2%
	Linearity	$\epsilon_{\text{CO}_2,\text{lin}}$	1%
	Span Drift	$\epsilon_{\text{CO}_2,\text{span}}$	2%
	Gas Accuracy	$\epsilon_{\text{CO}_2,\text{gas}}$	2%
Other	Distance	$\epsilon_d$	4%
	Time Delay	$\epsilon_t$	3%
	Environmental Conditions	$\epsilon_B$	0%
	CSV	$\epsilon_{\text{CSV}}$	3%
Zero Drift	Analyzer zero Drift	$\delta_{\text{drift}}$	0%